IET Renewable Power Generation

The Institution of Engineering and Technology | WILEY

ORIGINAL RESEARCH

Stochastic optimal power flow framework with incorporation of wind turbines and solar PVs using improved liver cancer algorithm

Noor Habib Khan[1] | Yong Wang[1] | Salman Habib[2,3] | Raheela Jamal[1] | Muhammad Majid Gulzar[2,4] | S. M. Muyeen[5] | Mohamed Ebeed[6,7]

[1]Department of New Energy, North China Electric Power University, Beijing, China

[2]Department of Control & Instrumentation Engineering, King Fahd University of Petroleum & Minerals, Dhahran, Saudi Arabia

[3]Interdisciplinary Research Center for Smart Mobility and Logistics, King Fahd University of Petroleum and Minerals, Dhahran, Saudi Arabia

[4]Interdisciplinary Research Center for Sustainability Energy Systems (IRC-SES), King Fahd University of Petroleum and Minerals, Dhahran, Saudi Arabia

[5]Department of Electrical Engineering, Qatar University, Doha, Qatar

[6]Electrical Department, Faculty of Electrical Engineering, Sohag University, Sohag, Egypt

[7]Department of Electrical Engineering, University of Jaén, Jaén, Spain

Correspondence

Salman Habib, Department of Control & Instrumentation Engineering, King Fahd University of Petroleum & Minerals, Dhahran, 31261, Saudi Arabia.
Email: salman.habib@kfupm.edu.sa

S.M. Muyeen, Department of Electrical Engineering, Qatar University, Doha, 2713, Qatar.
Email: sm.muyeen@qu.edu.qa

Abstract

The present study introduces a nature inspired improved liver cancer algorithm (ILCA) for solving the non-convex engineering optimization issues. The traditional LCA (t-LCA) inspires from the conduct of liver tumours and integrates biological ethics during the optimization procedure. However, t-LCA facing stagnation issues and may trap into local optima. To avoid such issues and provide the optimal solution, there are some modifications are implemented into the internal structure of t-LCA based on Weibull flight operator, mutation-based approach, quasi-opposite-based learning and gorilla troops exploitation-based mechanisms to enhance the overall strength of the algorithm to obtain the global solution. For validation of ILCA, the non-parametric and the statistical analysis are performed using benchmark standard functions. Moreover, ILCA is applied to resolve the stochastic renewable-based (wind turbines + PVs) optimal power flow problem using a modified RER-based IEEE 57-bus. The objective of this work is to obtain the minimum predicted power losses and enhance the predicted voltage stability. By incorporation of renewable resources into the modified IEEE57-bus network can help the system to reduce the power losses from 5.6622 to 3.8142 MW, while the voltage stability is enhanced from 0.1700 to 0.1164 p.u.

1 | INTRODUCTION

The OPF is a non-convex and utmost considerable optimization issue that received an extensive attraction of the utilities and especially of the researchers due to its secure and economic operation provided in electric power networks [1]. The problem is further multifaceted due to more effective ways being added to fulfil the energy requirements in modern power systems. These effective and feasible ways are possible via the incorporation of renewable resources. Though adding the uncertainties to electric networks forecast subsequent from the large incorporation of these resources, with increased complexity and size of the network have severely intricate the task of resolving the OPF problem [2].

The second major concern is the voltage stability that is taken into account for planning system design and operation. Consequently, new utilities organizations functioning the power transmission corridors near to the voltage stability parameters due to their profitable market point-of-view. Otherwise, this has directed to violation and cause of voltage collapse with high-cost penalties to both consumers and utilities. The impact of renewable on voltage stability has been discussed in [3].

In recent years, the researcher has tended to utilize optimization methods to resolve OPF problems since of their efficient response and ability to deal with the non-linear large-scale networks. These methods have wide-range categories that are inspired based on human, physics, evolutionary and nature swarm-based approaches [4]. In human-based, the algorithm imitates human conduct like socializing, competition, learning etc. Among these who fall under their category are teaching-learning-based optimization [5], Jaya algorithm [6], imperialist competition algorithm [7], skilled optimization algorithm [8] and so on. The physics-based algorithms mimic the natural and physical rules to obtain the solution. The improved gravitational search algorithm [9] mimics the perception of Newton's law in development, the lightning search algorithm [10] mimics the natural lightning marvels, the multi-verse algorithm [11] mimics the perception of cosmology contains worm, white and black-hole, and so on. The evolutionary-based algorithm mimics the evolutionary perception, where the finest solution is attained by offspring from parents' mating. Among these few are reported here like improved differential evolution [12], genetic algorithm [13], ensembled successive history adaptive differential evolutionary algorithm [14], adaptive guided differential evolution algorithm [15] and so on. The swarms-based on the other hand, that is inspired by the social response of the animals or groups as popularized like particle swarm optimization [16, 17] and chaotic particle swarm optimization [18, 19]. There are numerous swarm-based algorithms have been reported in the literature such as the grey-wolf optimizer [20], grasshopper optimization algorithm [21], moth-flame optimizer [22], kill-herd algorithm [23], pigeon-inspired optimization algorithm [24], gorilla troops optimizer [25] and so on.

Several probabilistic techniques were used to resolve the stochastic OPF problem large number of incorporation of WTs and solar PV units in the power system. These probabilistic methods can offer optimal solutions and adequate precision in the presence of uncertainties [26, 27]. Different related techniques such as cumulant, Monte-Carlo simulations (MCS) as well as probabilistic collocation approaches are extensively utilized to enumerate the influence of system uncertainties on the different aspects of the system with voltage stability as an objective [28]. The authors in [29], implemented the Cornish Fisher extension to tackle the uncertainty of PV, but the approach was not good enough to provide an optimal estimation for issues containing non-convex and complex structures return functions. The authors in [30], proposed two-point estimation (2PEM) technique based on the moments approach to deal with PV uncertainties. Though, the solution was untrustworthy due to generating estimates outside the parameters space and not having sufficient statistics to tackle the problem. The

authors in [31], deal with the stochastic OPF problem, where the Kernel density estimate approach was employed in approximating the PDF of windspeed. However, it depends on the initial position of bins, and they grow exponentially with dimensions which make it unpractical. The authors in [32], proposed a mean-variance-skewness model to resolve the stochastic OPF framework with the incorporation of wind power based on Latin hypercube sampling (LHS), but it suffered from loss of statistical sampling points and difficulty to deal with the arbitrary sampling practically for computational sensitivity analysis. The authors in [33], utilized MCS variants to reach the probability of the PDFs of generated power output by wind system. The authors in [34], used a genetic algorithm and two-point estimate techniques to resolve the OPF problem with the incorporation of wind and solar powers into the modified IEEE 30-bus network. The impact of uncertainties such as solar irradiance, wind speed and load variations were taken into the account during solution to the problem. The authors in [35], proposed the techno-economic analysis for the OPF problem coordinated with hybrid renewable resources like solar and wind energy using IEEE 30-bus network. Using the appropriate probability density methods such as Weibull and Lognormal PDFs to model the system uncertainty. The authors in [36], proposed a thermal exchange optimization algorithm based on Newton's law of cooling, to resolve the probabilistic OPF problem using both conventional and renewable energy sources via an IEEE 30-bus network. The system uncertainties such as solar PV and wind powers were taken into account using suitable PDFs for modelling. The authors in [37], used the ant lion optimization algorithm to resolve the OPF problem considering wind energy resources and to handle the wind speed uncertainty, the Weibull PDF approach was applied in the work. The authors in [38], used Weibull distribution to simulate the variation of wind speed and proposed the modified bacterial foraging algorithm to resolve the probabilistic OPF problem using an IEEE 30-bus network. The authors in [39], proposed the enhanced version of the adaptive differential evolution algorithm based on four modifications, crossover rate sorting mechanism, re-randomizing parameters, dynamic population reduction-based strategy and self-adaptive penalty constraints handling approach. The proposed EJADE-SP was further used to resolve the OPF problem with incorporation of solar, wind and thermal generation-based modified IEEE 30-bus network. The authors in [40], proposed an improved the version of skilled optimization algorithm based on the opposite-based learning (OBL) mechanism to resolve the stochastic OPF problem wind-based modified IEEE 30 and 57-bus networks. The authors in [41], proposed the whale optimization algorithm to resolve the stochastic OPF problem using hybrid resources. The uncertainty of solar and wind are modelled via lognormal and Weibull distributions. The authors in [42], resolve the multi-objective OPF problem using elitist non-dominated sorting genetic algorithm (NGSA-II and NGSA-III) with incorporation of wind energy into the Algerian 114 node-based network. The details of the studies presented to the literature to resolve the stochastic OPF problem compared to the current study are provided in Table 1.

TABLE 1   The details of the studies presented to the literature for solving the OPF problem.

Reference	Algorithm	RERs		Uncertain load demand	Bus network
		Wind	PV		
[5]	Teaching-learning-based optimization	✗	✗	✗	30-bus
[7]	Imperialist competitive algorithm	✗	✗	✗	57-bus
[9]	Improved gravitational search algorithm	✗	✗	✗	30, 57-bus
[10]	Lightning search algorithm	✗	✗	✗	30, 57-bus
[12]	Composite differential evolution integrating effective constrained handling techniques	✗	✗	✗	30, 57 and 118-bus
[14]	Ensembled successive history adaptive differential evolutionary algorithm	✗	✗	✗	30 and 118-bus
[20]	Grey-wolf optimizer	✗	✗	✗	57-bus
[22]	Moth-flame optimizer	✗	✗	✗	30 and 57-bus
[25]	Chaotic-quasi-oppositional-phasor based multi populations gorilla troop optimizer	✗	✗	✗	30, 57-bus
[34]	Genetic algorithm	✓	✓	✓	30-bus
[35]	Equilibrium optimizer	✓	✓	✗	30-bus
[36]	Thermal Exchange optimization	✓	✓	✗	30-bus
[37]	Antlion optimization	✓	✗	✗	30-bus
[38]	Modified bacterial foraging algorithm	✓	✗	✗	30-bus
[39]	Enhanced adaptive differential evolution with self-adaptive penalty constraint handling	✓	✓	✗	30-bus
[40]	Improved skill optimization algorithm		✗	✗	30, 57-bus
[41]	Whale optimization algorithm	✓	✓	✓	30-bus
[42]	Elitist non-dominated sorting genetic algorithm (NGSA-II and NGSA-III)	✓	✗	✗	Algerian 114-bus
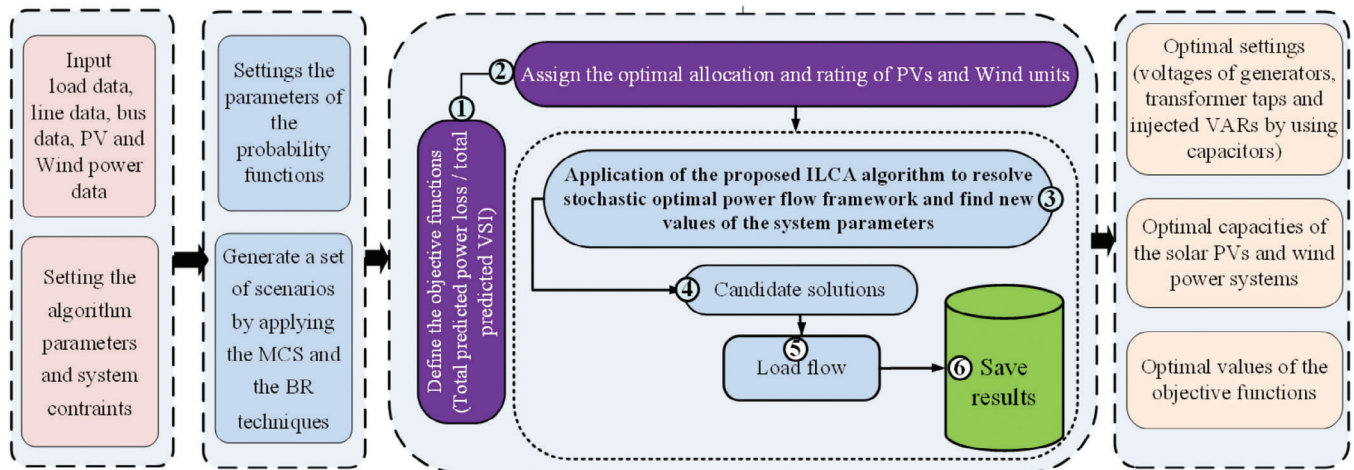
FIGURE 1   The proposed solution of the stochastic optimal power flow considering PV and wind power systems.

The main research gap is that solving the stochastic OPF problem with incorporation of solar PVs and wind energy units into the large-scale networks considering system uncertainties are becoming even more intricate problem and a robust optimization algorithm is required for solving this problem. The framework of the proposed study is illustrated in Figure 1. In the research, stochastic OPF problem is resolved while considering the uncertainties of the system such as time-varying load demand, WTs and solar PVs to minimize the total predicted power loss and enhance the total predicted voltage stability of

the large-scale IEEE 57-bus network. To avoid the stagnation issues in t-LCA, the four novel modifications are implemented in the research. The primary contributions of this research are given as follows:

➢ Four novel improvements are implemented into the internal structure of the traditional liver cancer algorithm (t-LCA) based on Weibull flight operator, mutation-based approach, quasi-opposite-based learning (QOBL) and gorilla troops exploitation-based mechanisms to enhance the exploration and exploitation strength of the algorithm.

➢ The proposed ILCA is further used to resolve the stochastic OPF problem by incorporation of two solar PVs and two wind energy units using a modified large-scale IEEE 57-bus network to obtain the least predicted power loss and enhance the system stability.

➢ Modelling the system uncertainties such as solar irradiance, wind speed and time-varying load demand via Lognormal, Weibull and normal distribution functions, while for creating the optimal set of uncertain scenarios the Monte-Carlo simulation (MCS) and the scenario-based reduction (SBR) techniques are used to accurately model the system uncertainties.

➢ Statistical and non-parametric analysis is executed using 23 standard benchmark functions to validate the effectiveness of the ILCA compared with the other traditional techniques such as SCSO, LAPO, ZOA, WOA and t-LCA.

For the easiness of the readers, the paper is arranged in different sections to understand well the follow of study. Sections 2 and 3 are the objective formulations for the stochastic OPF framework and also provide detailed methods to deal with the uncertainties in RERs. Section 4 is a methodology, where the modifications are implemented into the t-LCA algorithm. Section 5 presented the results and discussion of different cases of stochastic OPF objectives, while Section 6 is the part of the conclusion.

2 | OBJECTIVE FUNCTIONS OF OPF

In OPF, the objective function is achieved by adjusting the optimal values of power system variables to lessen the losses and enhance the voltage stability while satisfying the system constraints. The objective function of OPF is defined as follows:

$$lessen \; Obj\_Function \, (o, k) \quad (1)$$

Subjected to,

$$b_m (k, o) = 0 \; m = 1, 2, 3, \dots, i \quad (2)$$

$$l_n (k, o) \leq 0 \; n = 1, 2, 3, \dots, j \quad (3)$$

where b_m and l_n refer to the inequality and equality constraints, while, k and o are represented as state and control variables here.

These variables are formulated as follows:

$$k = [P_{G1}, V_{L1} \dots V_{LNPQ}, Q_{G1} \dots Q_{GNPV}, S_{TL1} \dots S_{TLNTL}] \quad (4)$$

$$o = [P_{G2} \dots P_{GNG}, V_{G1} \dots V_{GNG}, Q_{C1} \dots Q_{CNC}, T_1 \dots T_{NT}] \quad (5)$$

where V_L, S_{TL}, Q_G and P_{G1} are referred to the load-bus voltages, apparent power at transmission lines (T_L), active power produced by slack bus as well as reactive power produce by generator. While, Q_C, T, P_{G2} and V_G refer to shunt VAR compensators, transformer tap settings, power produced from generators and generator bus voltages.

2.1 | Total predicted power loss minimization

The first objective is to resolve the stochastic OPF problem to lessen the total predicted power loss, the related expression is given as follows [43].

$$Objective\_Function_1 = \text{Total\_PPL} = \sum_{n=1}^{Ngs} \text{PPL}_n = \sum_{n=1}^{Ngs} \pi_{r,n} \times P_{\text{Loss},n} \quad (6)$$

where $Total\_PPL$ and PPL_n are referred to the expected predicted power losses and at the nth scenario. P_{Loss} and Ngs referred to the power losses and the number of created scenarios, while, $\pi_{r,n}$ is n^{th} scenario probability.

$$P_{\text{loss}} = \sum_{i=1}^{N_L} G_{ij} (V_i^2 + V_j^2 - 2V_i V_j cos \delta_{ij}) \; (\text{MW}) \quad (7)$$

where V_j and V_i are the voltage at bus j and i, while δ_{ij} are G_{ij} the different of voltage angles and the T_L conductance.

2.2 | Enhancement of total predicted voltage stability

The second objective is to resolve the stochastic OPF problem to enhance the total predicted voltage stability index, the related expression is given as follows [28].

$$Objective\_Function_2 = \text{Total\_PVSI} = \sum_{n=1}^{Ngs} \text{PVSI}_n = \sum_{n=1}^{Ns} \pi_{r,n} \times \text{VSI}_n \quad (8)$$

where Total_PVSI and PVSl$_n$ are referred to the expected predicted voltage stability index at the nth scenario. Ngs is referred to the number of created scenarios, while, $\pi_{r,n}$ is referred to the nth scenario probability.

$$\text{VSI} = \min (L_{\max}) = \min \left(\max (L_j) \right) \forall j = 1, 2, \dots, N_{N_Q} \quad (9)$$

$$L_j = \left| 1 - \sum_{i=1}^{N_G} F_{ji} \frac{V_i}{V_j} \right| \forall j = 1, 2, \dots, NL \quad (10)$$

$$F_{ji} = -[Y_1]^{-1} [Y_2] \quad (11)$$

where Y_1 and Y_1 are the bus admittance metrices, while L_j is j^{th} line stability index.

2.3 | Constraints of the system

2.3.1 | Equality constraints

$$P_{Gi} - P_{Di} = |V_i| \sum_{j=1}^{NB} |V_j| \left(G_{ij}\cos\delta_{ij} + B_{ij}\sin\delta_{ij} \right) \quad (12)$$

$$Q_{Gi} - Q_{Di} = |V_i| \sum_{j=1}^{NB} |V_j| \left(G_{ij}\cos\delta_{ij} + B_{ij}\sin\delta_{ij} \right) \quad (13)$$

where G_{ij} and B_{ij} and are the conductance and susceptance, while P_{Gi}, P_{Di} and Q_{Gi}, Q_{Di} are the active and reactive generation of power and demand.

2.3.2 | Inequality constraints

The related constraints are given as follows:

$$P_{Gn}^{min} \leq P_{Gn} \leq P_{Gn}^{max} \quad n = 1, 2, \dots, NG \quad (14)$$

$$V_{Gn}^{min} \leq V_{Gn} \leq V_{Gn}^{max} \quad n = 1, 2, \dots, NG \quad (15)$$

$$Q_{Gn}^{min} \leq Q_{Gn} \leq Q_{Gn}^{max} \quad n = 1, 2, \dots, NG \quad (16)$$

$$T_n^{min} \leq T_n \leq T_n^{max} \quad n = 1, 2, \dots, NT \quad (17)$$

$$Q_{Cn}^{min} \leq Q_{Cn} \leq Q_{Cn}^{max} \quad n = 1, 2, \dots, NC \quad (18)$$

$$V_{Ln}^{min} \leq V_{Ln} \leq V_{Ln}^{max} \quad n = 1, 2, \dots, NQ \quad (19)$$

$$S_{Ln} \leq S_{Ln}^{max} \quad n = 1, 2, \dots, NL \quad (20)$$

where P_G, Q_G and V_G are referring to the maximum and lower limits of the active, voltage, reactive power generations. While, P_G, Q_G and V_L, T_n, Q_c and S_L are referring to the maximum and lower limits of the capacitor banks, tap setting of transformers, load-bus voltages and apparent power at T_L. While, NG, NT, NC, NL and NQ are the number of connected generators, transformers, capacitor banks, transmission lines and load connected. If there is some violation in the system, can be formulated as [44, 45]:

$$F_{Obj} = Objective_{Function1} + Objective\_Function_2$$

$$+ \alpha_1 \left(P_{G1} - P_{G1}^{Lim} \right)^2 + \alpha_2 \sum_{i=1}^{N_G} \left(Q_{Gi} - Q_{Gi}^{Lim} \right)^2$$

$$+ \alpha_3 \sum_{i=1}^{N_Q} \left(V_{Li} - V_{Li}^{Lim} \right)^2 + \alpha_4 \sum_{i=1}^{N_L} \left(S_{Ti} - S_{Ti}^{Lim} \right)^2 (21)$$

where $\alpha_1, \alpha_2, \alpha_3$ and α_4 are the penalty weight factors for reactive and active power generation and related values are chosen to 100, 100, 100,000, and 100, respectively.

3 | MODELING OF SYSTEM UNCERTAINTIES

In this work, solar and wind powers are measured as the source of energy. It should be mentioned here that according to the prior studies, the most commonly utilized approaches for modelling uncertainty of load demands, solar irradiance, and wind speed are normal (Gaussian), lognormal, and Weibull PDFs. These methods rely on acquiring a vast amount of data and comparing it to different sorts of PDFs. The best PDF is then selected, which includes all probabilistic data [46]. The detail discussion is given in below sub-sections.

3.1 | Time-varying load demand modelling

The uncertain load demand fluctuate over the time, so to tackle such behaviour, the normal PDF is utilized to model the time-varying demand, the related formulation is as follows [47].

$$f_{ld}(P_{ld}) = \frac{1}{\sigma_{ld}\sqrt{2\pi}} \exp\left[-\frac{(P_l - \mu_{ld})^2}{2\sigma_{ld}^2} \right] \quad (22)$$

where σ_{ld} and μ_{ld} are referring to the mean and standard values selected to 90 and 10, while P_{ld} is the loading used by normal PDF.

3.2 | Solar irradiation modelling

The solar radiation has a high degree of uncertainty that fluctuates as a function based on several factors such as season, month, and time of the day as well as environmental conditions. The PDF of the solar irradiation is optimally modelled by a lognormal PDF. The related formulation is as follows [48].

$$f_{sl}(G_{sl}) = \frac{1}{G_{sl}\sigma_{sl}\sqrt{2\pi}} \exp\left[-\frac{(\ln(G_{sl}) - \mu_{sl})^2}{2\sigma_{sl}^2} \right] \quad G_{sl} > 0 \quad (23)$$

where σ_{sl} and μ_{sl} are referring to the mean and standard values selected to 0.5 and 5.5. The solar PV power is produced by the following expression.

$$P_{RP}(G_S) = \begin{cases} P_{PR}\left(\frac{G_s^2}{G_{ssi} \times X_{ci}} \right) & for \ 0 < G_S \leq X_{ci} \\ P_{RP}\left(\frac{G_S}{G_{ssi}} \right) & for \ G_S \geq X_{ci} \end{cases} \quad (24)$$

(a) Loading percentage (%).
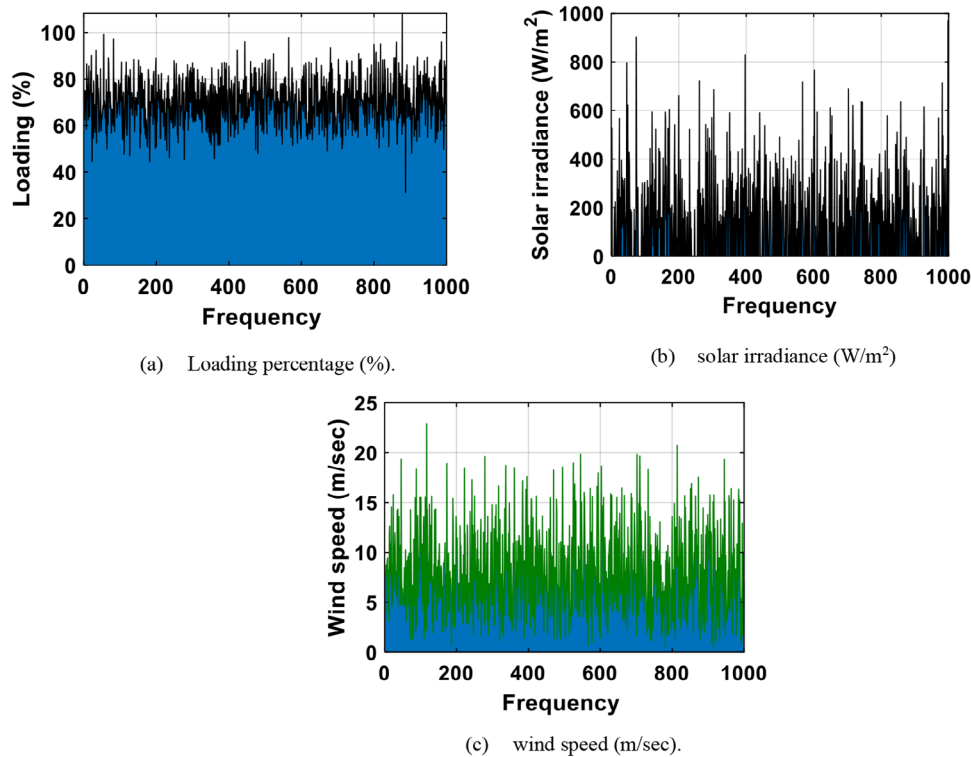
(b) solar irradiance (W/m²)

(c) wind speed (m/sec).

FIGURE 2 MCS and SBR-based approaches to model the load, the solar and the wind speed uncertainties at 1000 frequency.

where X_{ci} and G_{ssi} refer to the certain and standard solar irradiance values selected around 150 and 1000 W/m², respectively. In this study, the optimal allocated of two PV units rated 50 MW power capacity are connected on buses 16 and 26, respectively.

3.3 | Modelling of wind speed

The Weibull PDF approach is utilized to handle the wind speed (m/s) uncertainties, the expression is as follows [43].

$$f_u(u) = \left(\frac{\beta_{sp}}{\alpha_{sl}}\right)\left(\frac{u}{\alpha_{sl}}\right)^{(\beta_{sp}-1)} \exp\left[-\left(\frac{u}{\alpha_{sl}}\right)^{\beta_{sp}}\right] \quad 0 \leq u < \infty \tag{25}$$

where β_{sp} and a_{sl} are referring to the scale and shape parameters values selected to 10 and 2 [49]. The wind power is produced by the following expression.

$$P_{ws}(u_{ws}) = \begin{cases} 0 & \text{for } (u_{\omega s} \langle u_{\omega si} \& u_{\omega s} \rangle u_{\omega so}) \\ P_{RP}\left(\frac{u_{\omega s}-u_{\omega si}}{u_{\omega sr}-u_{\omega si}}\right) & \text{for } (u_{\omega si} \leq u_{\omega s} \leq u_{\omega sr}) \\ P_{RP} & \text{for } (u_{wsr} < u_{ws} \leq u_{wso}) \end{cases} \tag{26}$$

where $u_{\omega sr}$, $u_{\omega so}$ and $u_{\omega si}$ are referred as the rated, cut-in and out wind speed. In the study, the optimal allocation of two wind turbine units rated 90 MW power capacity are connected on buses 45 and 36, respectively.

The MCS and SBR techniques are used to create the uncertain scenarios, where the frequency is adjusted to 1000 and illustrated in Figure 2.

TABLE 2 MCS and RBS-based to model the uncertain load demand, solar irradiance and wind speed at 1000 frequency.

Number of scenarios	Load demand (%)	Wind speed (m/sec)	Solar irradiance (W/m²)	Probability
1	67.7366	12.5700	827.8942	0.0010
2	64.3277	6.0248	537.4406	0.0250
3	76.2579	8.6338	718.4929	0.0070
4	66.1736	5.5602	0.0000	0.5030
5	70.4822	5.4440	191.6005	0.2440
6	69.9016	3.0197	1490.6640	0.0010
7	70.1290	12.7045	292.6203	0.1130
8	65.6065	10.5367	614.7596	0.0140
9	67.7204	4.4658	361.9548	0.0900
10	69.2140	10.0340	969.4503	0.0020

The ten optimal scenarios are created for uncertain varying demand, the wind speed and the solar irradiance as well as their corresponding probabilities are tabulated in Table 2.

4 | METHODOLOGY

In this section, a novel bio-inspired optimization traditional method named liver cancer algorithm (t-LCA) is modified via four novel tactics such as Weibull flight operator,

mutation-based approach, gorilla troops exploitation-based approach and combination of quasi with opposite-based learning (QOBL) techniques are imposed to enhance the strength of t-LCA. The related formulation with descriptions of t-LCA and proposed ILCA are provided in the following sub-sections.

4.1 | Traditional liver cancer algorithm (t-LCA)

This sub-section defines the traditional t-LCA with detailed formulation. It inspires from the conduct of liver tumours and integrates biological ethics during the optimization procedure [50]. In t-LCA, the mimic spread and malignant growth of tumours can cause of worst effects on body and to imitate their behaviour, the algorithms contain several steps and related formulations as:

4.1.1 | Tumour size approximation

In this stage, the mathematical model is based on supposed to have a tumour with hemi-ellipsoid shape and determine their size to observe by length, height and width. The initial position is calculated by using the random opposition-based learning (ROBL) method, can be formulated as:

$$
X_i^{0j} = \frac{\pi}{6} \left(Le^j \right) \cdot \left(Wi^j \right) \cdot \left(Hi^j \right) - \left(lb + (ub - lb) - r_d \times X_i^j \right) \tag{27}
$$

where X_i^{0j} is a vector that opposite to X_i^j, r_d refers to random values range 0 to 1, lb and ub are the lower and upper limits, while Le, Hi and Wi are referring to the diameter of the tumour. The rise in tumour size is formulated as:

$$
X = \frac{\pi}{6} \cdot f \cdot (Le \cdot Wi)^{3/2} \tag{28}
$$

where f is equals to 1.

4.1.2 | Tumour recurrence

In this stage, hepatocellular carcinoma has growth exponentially due to developed of tumour in numerous locations in liver, so the location of tumours is as follows:

$$
P^i = \frac{dV}{dt} = r \times X \in [1 \dots T] \text{ and } i \in [1 \dots N] \tag{29}
$$

where T and N are referring to the number of maximum iterations and populations, while P is the growth tumor location. Here, Levy flight (LF) is imposed to locate the feast of tumour in liver.

$$
v(D) = 0.01 \times \frac{\text{rand } (1, D) \times \sigma}{|\text{rand } (1, D)|^{\frac{1}{\beta}}} \tag{30}
$$

$$
= \left(\frac{\Gamma(1 + \beta) \times \sin\left(\frac{\pi\beta}{2}\right)}{\Gamma\left(\frac{1+\beta}{2}\right) \times \beta \times 2^{\left(\frac{\beta-1}{2}\right)}} \right)^{\frac{1}{\beta}} \tag{31}
$$

The t-LCA uses the tumour growth mechanism and select the optimal part to access the situation in liver and determine the next process, expressed as follows:

$$
y = X + P \tag{32}
$$

$$
Z = Y + S \times LF(D) \tag{33}
$$

$$
X_{t+1}^i = \begin{cases} y \text{ if fit } (y) < fit\left(X_t^i\right) \\ z \text{ if fit } (z) < fit\left(X_t^i\right) \end{cases} \tag{34}
$$

where fit, S and D are referring to fitness function, random vector [0 to 1] and dimension of problem.

4.1.3 | Spreading of tumour

In this final stage, it is intellectualized of tumour spreading into the other part of organ, for such purpose to know the state, two operators are introduced such as crossover and mutation. In mutation process, mutation rate (ϵ) is used to update the location of the populations where the two vectors z and y to update old vector locations if random values are lower to ϵ, which is expressed as follows:

$$
y_{\text{Mut}} = \begin{cases} X & \text{if } r_1 \geq \epsilon \\ y & \text{else} \end{cases} \tag{35}
$$

$$
z_{\text{Mut}} = \begin{cases} X & \text{if } r_2 \geq \epsilon \\ z & \text{else} \end{cases} \tag{36}
$$

In which,

$$
\epsilon = \frac{t}{T}; \tag{37}
$$

$$
y = | X - X_i^j | \tag{38}
$$

$$
z = y - S \tag{39}
$$

where S contains D essentials selected from 0 to 1 range. While, in crossover, a novel vector is created by two entities, given as follows:

$$
X_{\text{Cross}} = \tau \times y_{Mut} + \left(1 - \tau'\right) \times z_{Mut}, \tau \neq \tau' \tag{40}
$$

where τ and τ' are the arbitrary vectors. The locations of the novel tumours are updated conferring to the fitness functions, given as follows:

$$
X_{t+1}^i = \begin{cases} y_{Mut} \text{ if fit } (y_{\text{Mut}}) < \text{fit}\left(X^i\right) \\ z_{Mut} \text{ if fit } (z_{\text{Mut}}) < \text{fit}\left(X^i\right) \\ X_{\text{Cross}} \text{ if fit } (w_{\text{Cross}}) < \text{fit}\left(X^i\right) \end{cases} \tag{41}
$$

4.2 | Modified lever cancer algorithm (ILCA)

In this sub-section, the novel modifications in t-LCA are presented which are based on four strategies such as Weibull flight operator, mutation-based approach, quasi-opposite-based learning (QOBL) and gorilla troops exploitation-based mechanisms. These novel modifications are applied to t-LCA to increase its overall exploration and exploitation strength as well as avoid of stagnations issue and reach to the global solution.

In the first step, the t-LCA is modified with Weibull flight operator where the cumulative Weibull is composed based on scale and shape factors, related expression is as follows:

$$f(x) = \left(\frac{\text{shape}}{\text{scale}}\right) \times \left(\frac{x}{\text{scale}}\right)^{(v-1)} \times e^{-(x/\text{scale})^{\text{shape}}} \text{ for } x \geq 0 \tag{42}$$

These scale and shape factors can be extracted from the Weibull distribution with wide and short step movements, where the wide step is expressed as follows:

$$\text{Step} = wblrnd(1, 1, [1, D]) \times sign(rand(1, D) - 0.5) \tag{43}$$

where, *sign* provides the values range $[-1,1]$ and *wblrnd* refers to the random number generated from Weibull distribution. While, the short step is expressed as follows:

$$\text{Step} = \begin{cases} wblrnd(0.5, 1, [1, D]) \times 0.5 \times sign(rand(1, D) - 0.5) \\ \times norm(x_{bst} - x_i), \text{ if } x_{bst} \neq x_i \\ wblrnd(0.5, 1, [1, D]) \times 0.1 \times sign(rand(1, D) - 0.5), \text{ else} \end{cases} \tag{44}$$

The new generated populations' position that is formulated as:

$$x_{\text{new},i} = x_{\text{new},i} + \text{Step} \tag{45}$$

In the second step, the mutation strategy is employed for gentote a new mutant vector for each population for improving the exploration process of the ILCA algorithm. Two frequently mutation strategies are used, which can be applied as follows [51, 52]:

$$if \ rand > 0.5$$

$$x_{\text{new},i} = x_{r1} + F(x_{r2} - x_{r3}) \tag{46}$$

$$else$$

$$x_{\text{new},i} = x_i + F(x_{\text{best}} - x_i) + F(x_{r1} - x_{r2}) \tag{47}$$

$$end$$

where, the r_1, r_2 and r_3 are random integers created from set of $\{1, 2, \ldots, NP\}$.

In the third step, the gorilla troops exploitation tactic is imposed to boost the exploitation strength of the t-LCA

algorithm. The location is updated based on the following formulation.

$$Gx_i(t+1) = L \times M \times (x_i(t) - x_{\text{prey}}(t)) + X(t) \tag{48}$$

$$M = \left(\left|\frac{1}{N}\sum_{i=1}^{N} Gx_i(t)\right|^g\right)^{\frac{1}{8}} \tag{49}$$

$$g = 2^L \tag{50}$$

If the condition is condition is not satisfied, then update the position settlement based as follows.

$$G x_i = x_{\text{prey}}(t) - (x_{\text{prey}}(t) \times Q - x_i \times Q) \times A \tag{51}$$

$$Q = 2 \times r_5 - 1 \tag{52}$$

$$A = \beta \times E \tag{53}$$

$$E = \begin{cases} N_1, \text{ rand} \geq 0.5 \\ N_2, \text{ rand} < 0.5 \end{cases} \tag{54}$$

where, E and β are the random and predetermined values in normal distribution, while r_5 is the random value range 0 to 1.

In the fourth step, the quasi-opposite-based learning (QOBL) approach, the quasi signifies the centre of the search area (SA), while OBL is referred to the choice of a point in a reflected mirror point [53, 54], the expression is as follows:

$$\begin{aligned} &\boldsymbol{For} \ i = 1 \ : \ No. \ rabbits \\ &\quad \boldsymbol{For} \ j = 1 \ : \ D \\ &\quad\quad x_{i,j}^o = x_j^{\min} + x_j^{\max} - X_{i,j} \\ &\quad\quad c_{i,j} = \left(x_j^{\min} + x_j^{\max}\right)/2 \\ &\quad\quad \boldsymbol{If} \ (x_{i,j} < c_{i,j}) \\ &\quad\quad\quad x_{i,j}^{qo} = c_{i,j} + \left(x_{i,j}^o - c_{i,j}\right) \times rand \\ &\quad\quad \boldsymbol{else} \\ &\quad\quad\quad x_{i,j}^{qo} = c_{i,j} + \left(c_{i,j} - x_{i,j}^o\right) \times rand \\ &\quad\quad \boldsymbol{end} \\ &\quad \boldsymbol{end} \\ &\boldsymbol{end} \end{aligned} \tag{55}$$

The flow chart of stochastic OPF framework solved by using ILCA via modified RERs-based modified IEEE 57-bus is illustrated in Figure 3.

5 | RESULTS AND DISCUSSION

In present article, single-objective OPF cases have been considered without and with installation of multiple solar PVs and wind turbines using modified RERs-based IEEE 57-bus standard. The execution of simulations for the entire cases are performed on operating system PC core i9-13900H CPU @2.60 GHz 32GB RAM on MATLAB software version
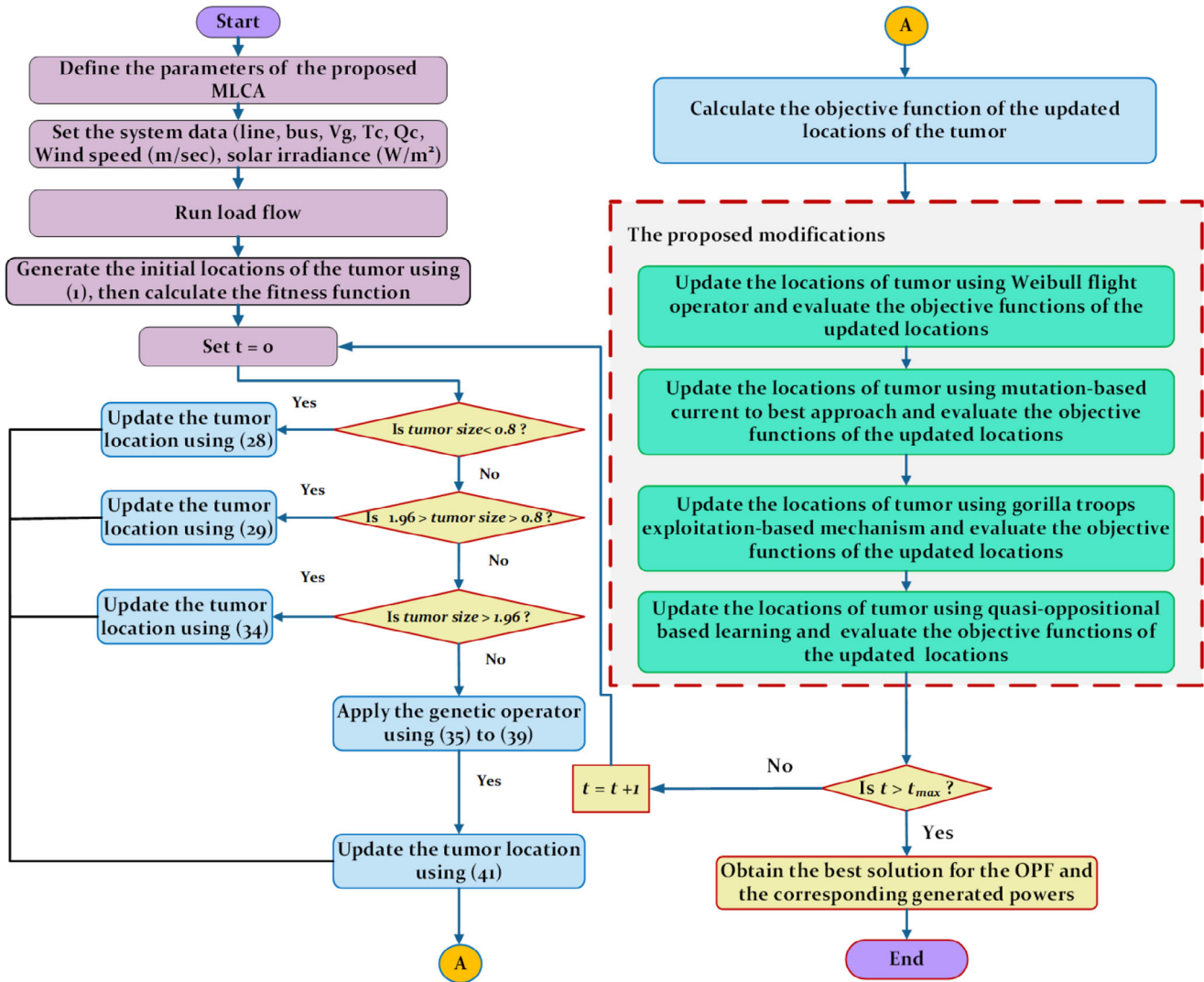
FIGURE 3 Flow chart of stochastic OPF framework solved by using improved liver cancer algorithm (ILCA) via modified RERs-based modified IEEE 57-bus.

R2023a. These objectives are investigated to access the implementation of the novel established method in accumulation to the judgment for other methods. To accept the performance and robustness of the proposed ILCA, the modified RERs-based IEEE 57-bus standard are carefully studied in the work. The simulations parameters such as number of populations, runs, iterations as well as other optimization settings for well-known optimizers including ILCA are tabulated in Table 3.

It should be highlighted here that the parameters of the proposed ILCA have been adjusted by 25 times running of this algorithm. The importance of this act is having compromise between best solution and run time. To validate the performance of ILCA, the unimodal, the multi-modals and the fixed dimensional 23 benchmark functions are added to the study. Moreover, the Wilcoxon and the Friedman non-parametric tests are applied to the algorithm to better observed the significance difference between ILCA and other aforementioned techniques. The detail about the statistical study analysis and OPF optimization engineering study with RERs are provided in the following sections.

5.1 | Standard benchmark functions

In this section, the information related to the 23 unimodal, the multi-modal and the fixed dimensional multi-modal functions [59, 60] used to carry out the statistical and non-parametric analysis to verify the effectiveness of ILCA over to other traditional optimization techniques. The detail of these functions is provided in the Appendix part, where these functions are divided into three Tables Appendix Tables A1, A2 and A3, according to their category such as unimodal, multi-modal and fixed dimensional functions.

Statistical analysis: The simulations are carried out by using the optimization parameters of the different algorithms provided in Table 3. To conduct a fair comparison, the parameters such as iterations, population and number of runs are adjusted the same. The statistical results of these functions are provided in Table 4, with best, average, worst, standard and time (s). By careful analysis of Table 4, it is readily apparent that an improved version of LCA, named "ILCA" provides an exceptional presentation of almost in entire spectrum of the

TABLE 3 The selected parameters of the studied optimizers.

Algorithms	For optimal power flow problem IEEE 57	For statistcal analysis
SCSO [55]	$t_{MAX} = 100$, Search Agent = 20, Runs = 25	$t_{MAX} = 200$, Search Agent = 20, Runs = 25
LAPO [56]	$t_{MAX} = 100$, Search Agent = 20, Runs = 25	$t_{MAX} = 200$, Search Agent = 20, Runs = 25
WOA [20]	$t_{MAX} = 100$, Search Agent = 20, Runs = 25	$t_{MAX} = 200$, Search Agent = 20, Runs = 25
ZOA [57]	$t_{MAX} = 100$, Search Agent = 20, Runs = 25	$t_{MAX} = 200$, Search Agent = 20, Runs = 25
EEFO [58]	$t_{MAX} = 100$, Search Agent = 20, Runs = 25	$t_{MAX} = 200$, Search Agent = 20, Runs = 25
LCA [50]	$t_{MAX} = 100$, Search Agent = 20, Runs = 25	$t_{MAX} = 200$, Search Agent = 20, Runs = 25
Proposed ILCA	$t_{MAX} = 100$, Search Agent = 20, Runs = 25, $aa = 4$, $zz = 0.1$, $p = 0.03$, $beta = 3$, $w = 0.8$	$t_{MAX} = 200$, Search Agent = 20, Runs = 25, $aa = 4$, $zz = 0.1$, $p = 0.03$, $beta = 3$, $w = 0.8$

benchmark functions. ILCA consistently secures a high rank almost in all given functions that refer to the remarkable performance attained by the ILCA over to the given traditional techniques like SCSO, LAPO, ZOA, WOA and traditional LCA.

Wilcoxon rank-sum test: It is the non-parametric test that is used to distinguish the significance difference among the algorithms. The P-values refer to the complex distribution values of the Wilcoxon analysis given in Table 5, among the proposed ILCA and other optimization algorithms. By jugging the outcomes given in Table 5, the proposed ILCA outperformed almost in entire functions, that is evident to prove the effectiveness of the ILCA better than other traditional techniques.

Convergence analysis: Figure 4, provides the rate of convergence curves behaviour of ILCA and other competitors that is obtained against each benchmark function to know the optimal response to obtain the global solution. By observing the convergence response, the proposed ILCA outperformed almost entire functions with a fast convergence rate to achieve the optimal solution. The results disclosed the robustness, effectiveness and efficacy of the ILCA over to other state-of-the-art techniques.

Friedman test: It is considered as the non-parametric test used to analyse the mean act of the algorithm on individual dataset, and then compare the mean sum of the other algorithm datasets to identify the significance difference among these algorithms in terms of getting an optimal mean response. The Friedman test illustration is shown in Figure 5, where the optimal values of the significance are attained by the pro-

posed ILCA, while the worst mean values are reported by the traditional LCA. It is mentioned here that the proposed modifications applied to the proposed ILCA improved the overall performance of the traditional LCA and other optimization techniques. By observing Figure 5, the traditional LCA is provided the worst mean response in the test.

5.1.1 | Solution to the OPF with RERs to obtain the minimum power losses and improve stability

In this section, to resolve the OPF solution using RERs to lessen the expected power loss and improve voltage stability using RER-based modified IEEE 57-bus. The reactive and the active power demands of the IEEE 57-bus are 336.4 MVAr and 1250.8 MW, while their bus data as well as line data can be found in [61]. The IEEE57-bus system contains 80 branches, 57 buses, 7 generators, 17 tap ratio and 3 shunt capacitors, respectively. The two solar PV and two wind farms are connected at bus 45, 36 and 16, 26, respectively. In the study, normal, lognormal and Weibull PDFs are used to tackle the system uncertainty like the load demand, the solar irradiance and the wind speed. Moreover, the MCS and SBR techniques are also implemented to create the 10 optimal scenarios for these uncertainties, which are tabulated in Table 2. The discussion related to OPF's corresponding objectives is provided in detail in the below sub-sections.

5.1.2 | Lessen the total predicted power loss (TPPL) without and with renewable resources

The first objective is to minimize the TPPL without and with the installation of multiple solar PV and wind turbines in the system. The convergence behaviour and the boxplot response are illustrated in Figure 6a,b to attain the objective function with SCSO, LAPO, WOA, ZOA, t-LCA and ILCA without considering RERs. The lowest optimal value is attained by the application of ILCA around 5.6622 MW, while t-LCA gives the worst response. The second and third columns of Table 6, shown here that the values of power losses and predicted power loss is attained against the time-varying load for each scenario.

Similarly, Figure 6a,b shows the convergence and boxplot responses for objective function with SCSO, LAPO, WOA, ZOA, t-LCA and ILCA considering with optimal presence of Solar PV and wind powers in the system. By jugging Tables 6 and 7, it is observed that the optimal response is attained by ILCA to lessen the TPPL objective reported around 3.8142 MW, while the worst values of TPPL are reported by the t-LCA algorithm. The overall saving in TPPL objective is reported around 32.6375% by inclusion of RERs. The optimal response of the two PVs and two connected windfarms are illustrated in Figure 6g–j, while the system response related to power generation, tap positions, generator voltages, shunt power capacitors, reactive generation limits as well as voltage magnitude responses are illustrated in Figure 6c–f,k,l, respectively. By seeing the

TABLE 4 Statistical results using 23 benchmark functions.

Function	Algorithm	Avg	Best	Worst	Std	Time
F1	SCSO	3.75×10^{-39}	1.49×10^{-48}	9.11×10^{-38}	1.82×10^{-38}	5.362761
	LAPO	1.38×10^{-6}	7.11×10^{-9}	7.59×10^{-6}	1.8×10^{-6}	0.712758
	WOA	7.54×10^{-22}	8.48×10^{-29}	6.58×10^{-21}	$1.77 \times 10^{-21}1$	0.333143
	ZOA	2.8×10^{-95}	2×10^{-99}	4.37×10^{-94}	9.33×10^{-95}	0.264218
	LCA	1.12×10^{-63}	2.7×10^{-194}	2.79×10^{-62}	5.59×10^{-63}	4.214285
	ILCA	1.81×10^{-64}	7.3×10^{-99}	4.53×10^{-63}	9.07×10^{-64}	4.331494
F2	SCSO	1.17×10^{-22}	8.69×10^{-26}	1.75×10^{-21}	3.55×10^{-22}	5.237495
	LAPO	0.000111	2.3×10^{-5}	0.000305	6.63×10^{-5}	0.861541
	WOA	2.54×10^{-18}	1×10^{-22}	2.68×10^{-17}	5.77×10^{-18}	0.373301
	ZOA	9.37×10^{-51}	2.05×10^{-54}	1.76×10^{-49}	3.49×10^{-50}	0.314574
	LCA	3.03×10^{-24}	1.41×10^{-89}	7.58×10^{-23}	1.52×10^{-23}	4.617885
	ILCA	2.84×10^{-22}	2.26×10^{-96}	7.1×10^{-21}	1.42×10^{-21}	4.444975
F3	SCSO	5.42×10^{-34}	6.86×10^{-44}	1.32×10^{-32}	2.63×10^{-33}	5.89459
	LAPO	0.036287	0.001814	0.176749	0.04125	2.309601
	WOA	97,388.34	33,505.72	153,325.6	27,046.02	1.075584
	ZOA	9.88×10^{-55}	2.12×10^{-67}	1.79×10^{-53}	3.73×10^{-54}	1.800924
	LCA	1.01×10^{-64}	1.8×10^{-166}	2.22×10^{-63}	4.46×10^{-64}	11.06211
	ILCA	9.03×10^{-62}	2.1×10^{-87}	2.26×10^{-60}	4.52×10^{-61}	10.65624
F4	SCSO	2.84×10^{-19}	2.68×10^{-24}	2.21×10^{-18}	5.89×10^{-19}	5.295813
	LAPO	0.000625	0.000185	0.001512	0.000359	0.911114
	WOA	57.7204	2.775497	92.1395	28.74049	0.343618
	ZOA	7.25×10^{-44}	7.3×10^{-49}	6.19×10^{-43}	1.65×10^{-43}	0.316654
	LCA	5.64×10^{-28}	1.5×10^{-109}	1.41×10^{-26}	2.82×10^{-27}	4.529686
	ILCA	1.73×10^{-28}	4×10^{-110}	4.17×10^{-27}	8.33×10^{-28}	4.329944
F5	SCSO	28.28763	26.52781	28.88022	0.751302	5.486749
	LAPO	27.46459	26.22006	28.75541	0.637181	1.093561
	WOA	28.73687	28.50423	28.85614	0.114297	0.489207
	ZOA	28.78693	28.53526	28.90902	0.114722	0.480531
	LCA	3.27005	0.001115	26.98392	8.731117	5.02946
	ILCA	0.052553	2.32×10^{-5}	0.414365	0.10343	4.925109
F6	SCSO	2.796459	0.69041	3.677968	0.602058	5.210308
	LAPO	0.588683	0.250568	1.034807	0.208479	0.900433
	WOA	2.081498	0.849656	3.201628	0.601135	0.317473
	ZOA	4.203855	2.788633	4.933175	0.549793	0.283967
	LCA	0.000909	5.5×10^{-5}	0.004686	0.00117	4.339922
	ILCA	0.000598	6.66×10^{-6}	0.003545	0.000772	4.465885
F7	SCSO	0.000801	2.75×10^{-5}	0.002549	0.000731	5.684615
	LAPO	0.002201	0.000294	0.006286	0.001579	1.739794
	WOA	0.008376	0.000282	0.03416	0.007527	0.85584
	ZOA	0.000336	1.58×10^{-5}	0.000962	0.000255	1.205678
	LCA	0.000163	2.54×10^{-6}	0.000493	0.000132	8.209929
	ILCA	5.38×10^{-5}	8.43×10^{-6}	0.000166	4.26×10^{-5}	11.95616

(Continues)

TABLE 4 (Continued)

Function	Algorithm	Avg	Best	Worst	Std	Time
F8	SCSO	−6350.7	−7832.52	−4208.73	889.8639	5.411373
	LAPO	−4538.93	−5532.15	−3977.03	382.5685	1.126829
	WOA	−9443.19	−12,547.8	−5640.35	1959.311	0.405531
	ZOA	−5914.65	−7641.65	−4328.37	888.9944	0.636076
	LCA	−12,569.3	−12,569.5	−12,568.4	0.253219	5.318722
	ILCA	−12,569.4	−12,569.5	−12,568.8	0.167117	7.526737
F9	SCSO	0.000801	2.75×10^{-5}	0.002549	0.000731	5.684615
	LAPO	0.002201	0.000294	0.006286	0.001579	1.739794
	WOA	0.008376	0.000282	0.03416	0.007527	0.85584
	ZOA	0.000336	1.58×10^{-5}	0.000962	0.000255	1.205678
	LCA	0.000163	2.54×10^{-6}	0.000493	0.000132	8.209929
	ILCA	5.38×10^{-5}	8.43×10^{-6}	0.000166	4.26×10^{-5}	11.95616
F10	SCSO	4.44×10^{-16}	4.44×10^{-16}	4.44×10^{-16}	0.000000	5.248004
	LAPO	0.000173	3.61×10^{-5}	0.000848	0.000167	1.074041
	WOA	2.58×10^{-12}	1.11×10^{-14}	5.03×10^{-11}	9.99×10^{-12}	0.407543
	ZOA	4.44×10^{-16}	4.44×10^{-16}	4.44×10^{-16}	0.000000	0.323531
	LCA	4.44×10^{-16}	4.44×10^{-16}	4.44×10^{-16}	0.000000	4.857664
	ILCA	4.44×10^{-16}	4.44×10^{-16}	4.44×10^{-16}	0.000000	6.74378
F11	SCSO	0.000000	0.000000	0.000000	0.000000	5.442914
	LAPO	0.006235	9.62×10^{-9}	0.029424	0.010484	1.069217
	WOA	0.029945	0.000000	0.748637	0.149727	0.439495
	ZOA	0.000000	0.000000	0.000000	0.000000	0.50097
	LCA	0.000000	0.000000	0.000000	0.000000	5.317117
	ILCA	0.000000	0.000000	0.000000	0.000000	7.619709
F12	SCSO	0.198393	0.102341	0.384451	0.080399	6.396742
	LAPO	0.022057	0.002716	0.123561	0.029787	3.193417
	WOA	0.203099	0.019562	0.640062	0.150997	1.519036
	ZOA	0.362243	0.17068	0.523579	0.09407	2.704363
	LCA	4.89×10^{-6}	1.27×10^{-9}	2.23×10^{-5}	5.73×10^{-6}	15.24467
	ILCA	4.81×10^{-7}	1.75×10^{-8}	5.78×10^{-6}	1.19×10^{-6}	22.11645
F13	SCSO	2.650575	1.863412	2.98205	0.248656	8.18298
	LAPO	0.697029	0.059408	1.494674	0.388102	3.895734
	WOA	1.410424	0.551904	2.69086	0.494915	6.335172
	ZOA	2.389686	2.000544	2.820626	0.234187	15.06508
	LCA	5.6×10^{-5}	3.56×10^{-6}	0.000328	7.77×10^{-5}	39.20766
	ILCA	0.000443	5.79×10^{-8}	0.01099	0.002197	22.81679
F14	SCSO	7.641451	0.998004	12.67051	4.45993	3.135565
	LAPO	1.089449	0.998004	2.21484	0.307033	7.981795
	WOA	5.07525	0.998004	12.67051	4.073605	2.823629
	ZOA	3.089698	0.998004	10.76318	2.370862	9.540415
	LCA	1.037765	0.998004	1.992031	0.198805	21.92266
	ILCA	0.998004	0.998004	0.998004	1.83×10^{-16}	31.25136

(Continues)

TABLE 4 (Continued)

Function	Algorithm	Avg	Best	Worst	Std	Time
F15	SCSO	0.000593	0.000308	0.001765	0.000348	0.934057
	LAPO	0.000801	0.000307	0.006543	0.001247	0.417972
	WOA	0.001363	0.000334	0.009708	0.001867	0.163771
	ZOA	0.001263	0.000308	0.020363	0.003986	0.24436
	LCA	0.000307	0.000307	0.000307	3.91×10^{-12}	3.690855
	ILCA	0.000307	0.000307	0.000307	6.09×10^{-11}	5.075643
F16	SCSO	-1.03163	-1.03163	-1.03163	1.85×10^{-8}	0.59655
	LAPO	-1.03163	-1.03163	-1.03163	4.41×10^{-7}	0.433229
	WOA	-1.03163	-1.03163	-1.03163	3.1×10^{-7}	0.191886
	ZOA	-1.03134	-1.03163	-1.02437	0.001452	0.262712
	LCA	-1.03163	-1.03163	-1.03163	4.75×10^{-16}	3.473824
	ILCA	-1.03163	-1.03163	-1.03163	5.17×10^{-16}	4.934049
F17	SCSO	0.397888	0.397887	0.397889	4.65×10^{-7}	0.523313
	LAPO	0.397887	0.397887	0.397887	0.000000	0.335502
	WOA	0.39846	0.397888	0.40364	0.001154	0.146462
	ZOA	0.397887	0.397887	0.397888	1.99×10^{-7}	0.169445
	LCA	0.397887	0.397887	0.397887	0.000000	3.219576
	ILCA	0.397887	0.397887	0.397887	0.000000	4.352201
F18	SCSO	3.000151	3.00000	3.000534	0.000155	0.563165
	LAPO	3.00000	3.00000	3.00000	1.81×10^{-15}	0.258281
	WOA	4.196549	3.000001	32.86415	5.972418	0.126201
	ZOA	3.00007	3.00000	3.000521	0.000138	0.166133
	LCA	3.00000	3.00000	3.00000	4.09×10^{-15}	3.083114
	ILCA	3.00000	3.00000	3.00000	2×10^{-15}	4.376594
F19	SCSO	-3.86191	-3.86278	-3.85531	0.001603	0.850475
	LAPO	-3.86278	-3.86278	-3.86278	2.1×10^{-15}	0.49923
	WOA	-3.8359	-3.86278	-3.62214	0.052291	0.253793
	ZOA	-3.86009	-3.86278	-3.8502	0.003164	0.344881
	LCA	-3.86278	-3.86278	-3.86278	1.92×10^{-15}	3.962314
	ILCA	-3.86278	-3.86278	-3.86278	2.06×10^{-15}	5.551118
F20	SCSO	-3.2126	-3.32199	-2.84041	0.124688	1.329923
	LAPO	-3.24536	-3.322	-3.0895	0.079643	0.615407
	WOA	-3.13538	-3.31356	-1.83865	0.293751	0.23464
	ZOA	-3.28426	-3.32199	-3.1343	0.065215	0.329644
	LCA	-3.30773	-3.322	-3.2031	0.039432	4.072954
	ILCA	-3.31724	-3.322	-3.2031	0.023779	5.902864
F21	SCSO	-5.34829	-10.1525	-0.88098	2.484105	1.039753
	LAPO	-6.31957	-10.1532	-2.68286	2.818465	0.516818
	WOA	-6.88527	-10.0764	-2.53858	2.463857	0.260089
	ZOA	-8.82571	-10.1532	-2.67749	2.44738	0.369946
	LCA	-10.1532	-10.1532	-10.1532	1.31×10^{-12}	4.28884
	ILCA	-10.1532	-10.1532	-10.1532	3.59×10^{-15}	6.195228

(Continues)

TABLE 4 (Continued)

Function	Algorithm	Avg	Best	Worst	Std	Time
F22	SCSO	−4.92737	−10.4024	−0.90989	2.480293	1.021636
	LAPO	−8.92267	−10.4029	−3.89118	2.351258	0.69179
	WOA	−5.48894	−10.3978	−2.7192	2.582384	0.278735
	ZOA	−8.91298	−10.4029	−5.0869	2.43478	0.443476
	LCA	−10.4029	−10.4029	−10.4029	3.36×10^{-14}	4.680771
	ILCA	−10.4029	−10.4029	−10.4029	3.92×10^{-15}	6.532743
F23	SCSO	−6.14918	−10.5357	−0.94449	3.044711	1.127312
	LAPO	−9.09397	−10.5364	−3.81771	2.518509	0.863238
	WOA	−5.7548	−10.4635	−1.66702	2.980254	0.32262
	ZOA	−9.61868	−10.5364	−3.83541	2.156249	0.509249
	LCA	−10.5364	−10.5364	−10.5364	6.4×10^{-15}	5.058781
	ILCA	−10.5364	−10.5364	−10.5364	2.24×10^{-15}	6.99391

TABLE 5 Wilcoxon ranking sum test applied to 23 benchmarks among ILCA and other optimization techniques.

Function	SCSO versus ILCA	LAPO versus ILCA	WOA versus ILCA	ZOA versus ILCA	LCA versus ILCA	ILCA versus ILCA
F1	1.42000×10^{-9}	1.42000×10^{-9}	1.42000×10^{-9}	8.41940×10^{-2}	1.42000×10^{-9}	1.42000×10^{-9}
F2	1.31000×10^{-8}	1.42000×10^{-9}	1.42000×10^{-9}	7.85899×10^{-1}	1.31000×10^{-8}	2.57000×10^{-8}
F3	1.42000×10^{-9}	1.42000×10^{-9}	1.42000×10^{-9}	1.46000×10^{-8}	1.42000×10^{-9}	1.42000×10^{-9}
F4	1.42000×10^{-9}	1.42000×10^{-9}	1.42000×10^{-9}	3.97150×10^{-2}	1.42000×10^{-9}	1.42000×10^{-9}
F5	1.80000×10^{-9}	4.13000×10^{-9}	1.42000×10^{-9}	1.42000×10^{-9}	1.80000×10^{-9}	1.42000×10^{-9}
F6	1.42000×10^{-9}	1.42000×10^{-9}	1.42000×10^{-9}	1.42000×10^{-9}	1.42000×10^{-9}	1.42000×10^{-9}
F7	3.02000×10^{-5}	3.67000×10^{-9}	2.57000×10^{-9}	8.80900×10^{-3}	3.02000×10^{-5}	6.15000×10^{-7}
F8	1.42000×10^{-9}	1.42000×10^{-9}	1.42000×10^{-9}	1.42000×10^{-9}	1.42000×10^{-9}	1.42000×10^{-9}
F9	3.02000×10^{-5}	3.67000×10^{-9}	2.57000×10^{-9}	8.80900×10^{-3}	3.02000×10^{-5}	6.15000×10^{-7}
F10	n/a	9.73000×10^{-11}	9.73000×10^{-11}	n/a	n/a	n/a
F11	n/a	9.73000×10^{-11}	5.13100×10^{-3}	n/a	n/a	n/a
F12	1.42000×10^{-9}	1.42000×10^{-9}	1.42000×10^{-9}	1.42000×10^{-9}	1.42000×10^{-9}	1.42000×10^{-9}
F13	1.42000×10^{-9}	1.42000×10^{-9}	1.42000×10^{-9}	1.42000×10^{-9}	1.42000×10^{-9}	1.42000×10^{-9}
F14	1.17000×10^{-9}	1.57000×10^{-8}	2.14000×10^{-9}	8.28000×10^{-9}	1.17000×10^{-9}	9.89000×10^{-10}
F15	1.42000×10^{-9}	1.42000×10^{-9}	1.42000×10^{-9}	1.42000×10^{-9}	1.42000×10^{-9}	1.42000×10^{-9}
F16	1.87000×10^{-10}	6.95000×10^{-8}	1.87000×10^{-10}	4.06000×10^{-9}	1.87000×10^{-10}	4.60000×10^{-10}
F17	9.73000×10^{-11}	n/a	9.73000×10^{-11}	3.65000×10^{-10}	9.73000×10^{-11}	9.73000×10^{-11}
F18	1.39000×10^{-9}	2.13800×10^{-3}	1.39000×10^{-9}	1.77000×10^{-9}	1.39000×10^{-9}	1.35000×10^{-9}
F19	7.10000×10^{-10}	1.57680×10^{-2}	7.10000×10^{-10}	7.10000×10^{-10}	7.10000×10^{-10}	7.73000×10^{-10}
F20	8.44000×10^{-8}	4.87085×10^{-1}	8.44000×10^{-8}	7.43000×10^{-7}	8.44000×10^{-8}	2.18000×10^{-9}
F21	9.13000×10^{-10}	1.92000×10^{-5}	9.13000×10^{-10}	9.13000×10^{-10}	9.13000×10^{-10}	4.72000×10^{-10}
F22	1.13000×10^{-9}	4.30624×10^{-1}	1.13000×10^{-9}	1.13000×10^{-9}	1.13000×10^{-9}	3.89000×10^{-10}
F23	1.20000×10^{-9}	2.88516×10^{-1}	1.20000×10^{-9}	1.20000×10^{-9}	1.20000×10^{-9}	1.07000×10^{-9}

overall response, it is mentioned here that there is no violation in the system and all the bounds are within the permissible limits.

In detailed view of Table 7, ten uncertain scenarios have been predicted to find the TPPL objective functions as discussed. The second and the third column of Table 7 are about the power loss and the predicted power losses against the uncertain scenarios. The lowest TPPL loss is achieved in scenario number 1, where the maximum power contribution of solar PVs and wind energy are added to the system. While, the worst TPPL is recorded at the scenario number 4, where the zero contribution from the solar PV and minor contribution of power from the windfarms.
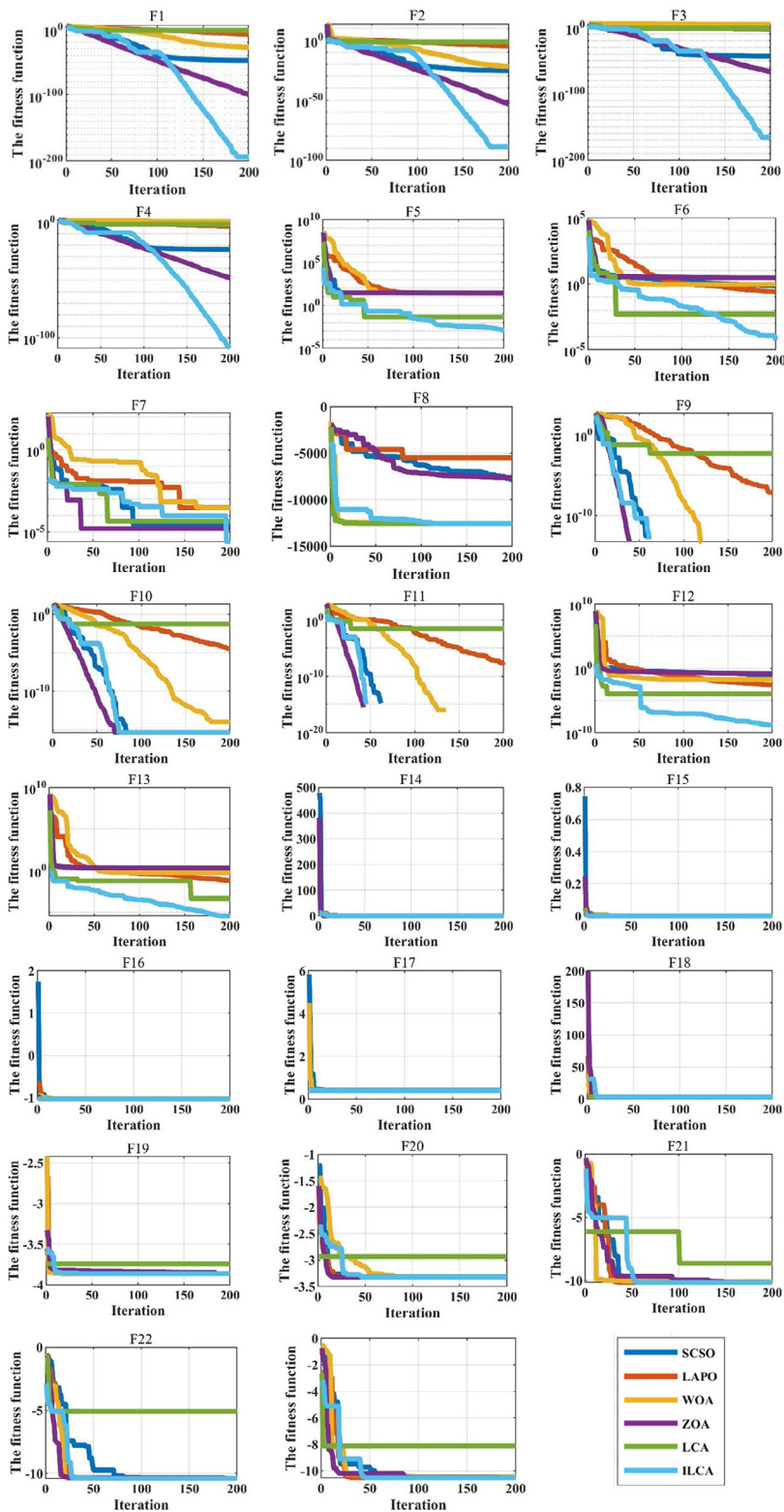
FIGURE 4 Convergence behaviour of improved liver cancer algorithm (ILCA) and other competitors' techniques via standard functions.

5.1.3 | Enhance the total predicted voltage stability (TPVSI) without and with renewable resources

The second objective is to enhance the TPVSI without and with installation of solar PV and wind powers into the system. The convergence behaviour and boxplot response are illustrated in Figure 7a,b to attain the objective function with SCSO, LAPO, WOA, ZOA, t-LCA and ILCA without considering RERs. The lowest optimal value of TPVSI is attained by the application of ILCA around 0.1700 p.u., while t-LCA gives the worst response. The fourth and fifth columns of Table 8, show here that the
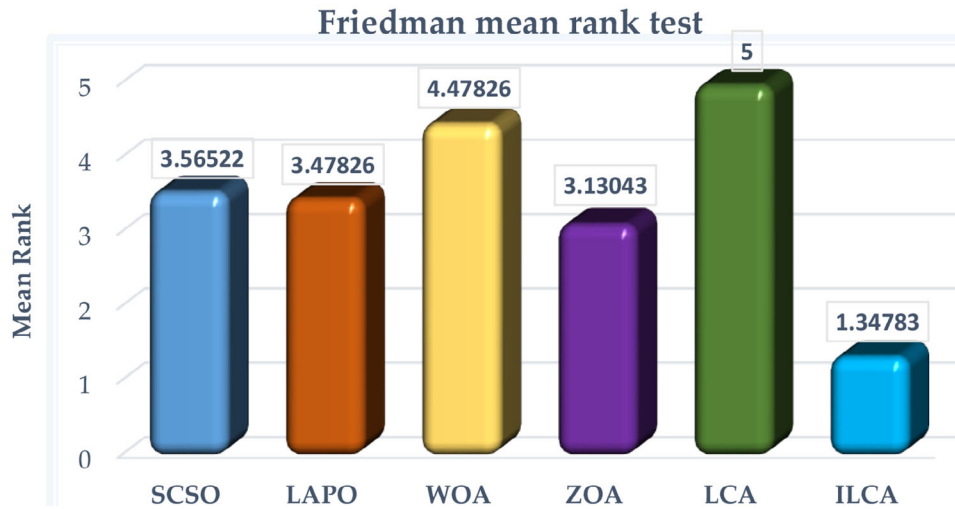
FIGURE 5 The Friedman mean test response compared with improved liver cancer algorithm (ILCA) and other competitors' techniques.

TABLE 6 The simulation results for objective of total predicted power loss (TPPL) without RESs.

Scenario	PL (MW)	TPPL (MW)	VSI (p.u)	TPVSI (p.u)
1	8.83091	0.00883	0.17232	0.00017
2	5.11611	0.12790	0.17002	0.00425
3	8.70078	0.06091	0.21086	0.00148
4	4.75704	2.39279	0.16571	0.08335
5	5.27398	1.28685	0.18139	0.04426
6	10.92638	0.01093	0.17298	0.00017
7	7.07471	0.79944	0.17964	0.02030
8	5.00231	0.07003	0.17414	0.00244
9	9.88407	0.88957	0.18320	0.01649
10	7.48258	0.01497	0.18427	0.00037
	TPPL (MW)	**5.6622 MW**	**TPVSI (p.u)**	**0.1733 p.u.**

TABLE 8 The simulation results for objective of total predicted voltage stability index (TPVSI) without RESs.

Scenario	PL (MW)	TPPL (MW)	VSI (p.u)	TPVSI (p.u)
1	13.491943	0.013492	0.171024	0.000171
2	9.923575	0.248089	0.169917	0.004248
3	8.499357	0.059496	0.184236	0.001290
4	10.376887	5.219574	0.167419	0.084212
5	13.490480	3.291677	0.171148	0.041760
6	5.692337	0.005692	0.182081	0.000182
7	12.223178	1.381219	0.179152	0.020244
8	13.004331	0.182061	0.172219	0.002411
9	7.430727	0.668765	0.167984	0.015119
10	12.208459	0.024417	0.167193	0.000334
	TPPL (MW)	**11.0945 MW**	**TPVSI (p.u.)**	**0.1700 p.u.**

TABLE 7 The simulation results for objective of total predicted power loss (TPPL) with RESs.

Number of Scenario	PL (MW)	TPPL (MW)	VSI (p.u)	TPVSI (p.u)
1	4.67644	0.004676	0.065819	0.000065
2	3.227364	0.080684	0.108929	0.002723
3	4.226982	0.029589	0.109987	0.000770
4	3.652258	1.837086	0.15018	0.075541
5	3.832939	0.935237	0.154515	0.037702
6	7.361063	0.007361	0.122753	0.000123
7	4.292699	0.485075	0.070918	0.008014
8	3.880605	0.054328	0.079328	0.001111
9	4.107266	0.369654	0.142448	0.012820
10	5.250287	0.010501	0.076964	0.000154
	TPPL (MW)	**3.8142 MW**	**TPVSI (p.u)**	**0.1390 p.u.**

values of voltage stability and predicted voltage stability is attained against the time-varying load for each scenario.

Similarly, Figure 7a,b shows the convergence and boxplot responses for objective function with SCSO, LAPO, WOA, ZOA, t-LCA and ILCA considering with optimal presence of Solar PV and wind powers into the system. By jugging Tables 8 and 9, it is observed that the optimal response is attained by ILCA to lessen the TPVSI objective reported around 0.1164 p.u., while the worst values of TPVSI is reported by t-LCA algorithm. The overall saving in TPVSI objective is reported around 31.5294% by inclusion of RERs. The optimal response of the two PVs and two connected windfarms are illustrated in Figure 7g–j, while the system response related to power generation, tap positions, generator voltages, shunt power capacitors, reactive generation limits as well as voltage magnitude responses are illustrated in Figure 7c–f,k,l, respectively. By seeing overall response, it is mentioned here that entire system constraints are within their limits without getting any violations.
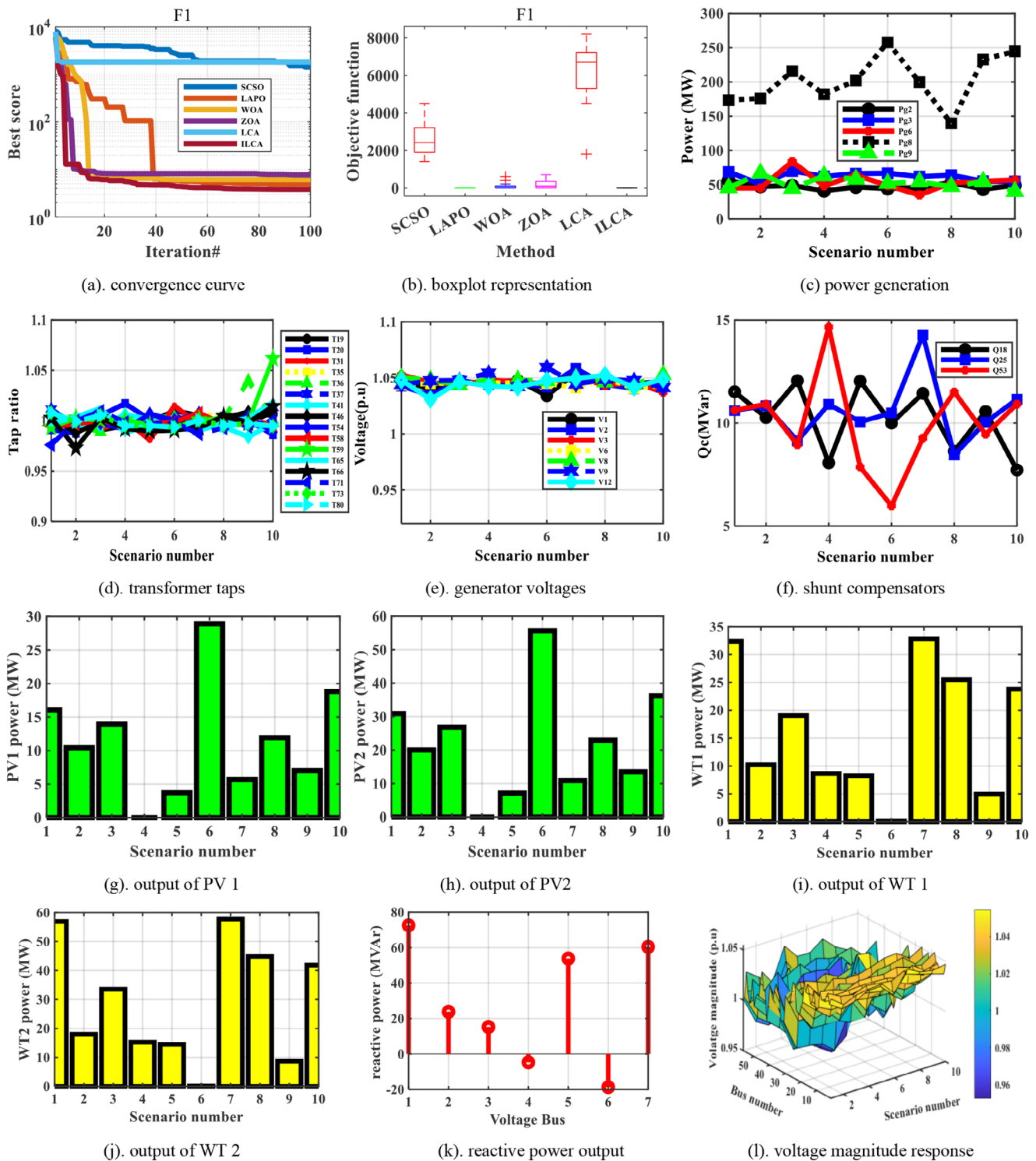
(a). convergence curve

(b). boxplot representation

(c) power generation

(d). transformer taps

(e). generator voltages

(f). shunt compensators

(g). output of PV 1

(h). output of PV2

(i). output of WT 1

(j). output of WT 2

(k). reactive power output

(l). voltage magnitude response

FIGURE 6　Lessen the total predicted power loss (TPPL) inclusion of wind and PV resources.

In detail view of Table 9, 10 uncertain scenarios have been predicted to find the TPSVI objective functions as discussed. The fourth and the fifth column of Table 9 is about the voltage stability and the predicted power losses against the uncertain scenarios. The lowest TPSVI is achieved at scenario number 1, where the maximum contribution of solar PV and wind energy are added into the system. While, the worst TPSVI is recorded at the scenario number 4, where the zero contribution from the solar energy as well as minor contribution recorded by the windfarms in the system.

(a). convergence curve

(b). boxplot representation

(c) power generation

(d). transformer taps

(e). generator voltages

(f). shunt compensators

(g). output of PV 1

(h). output of PV2

(i). output of WT 1

(j). output of WT 2

(k). reactive power output

(l). voltage magnitude response
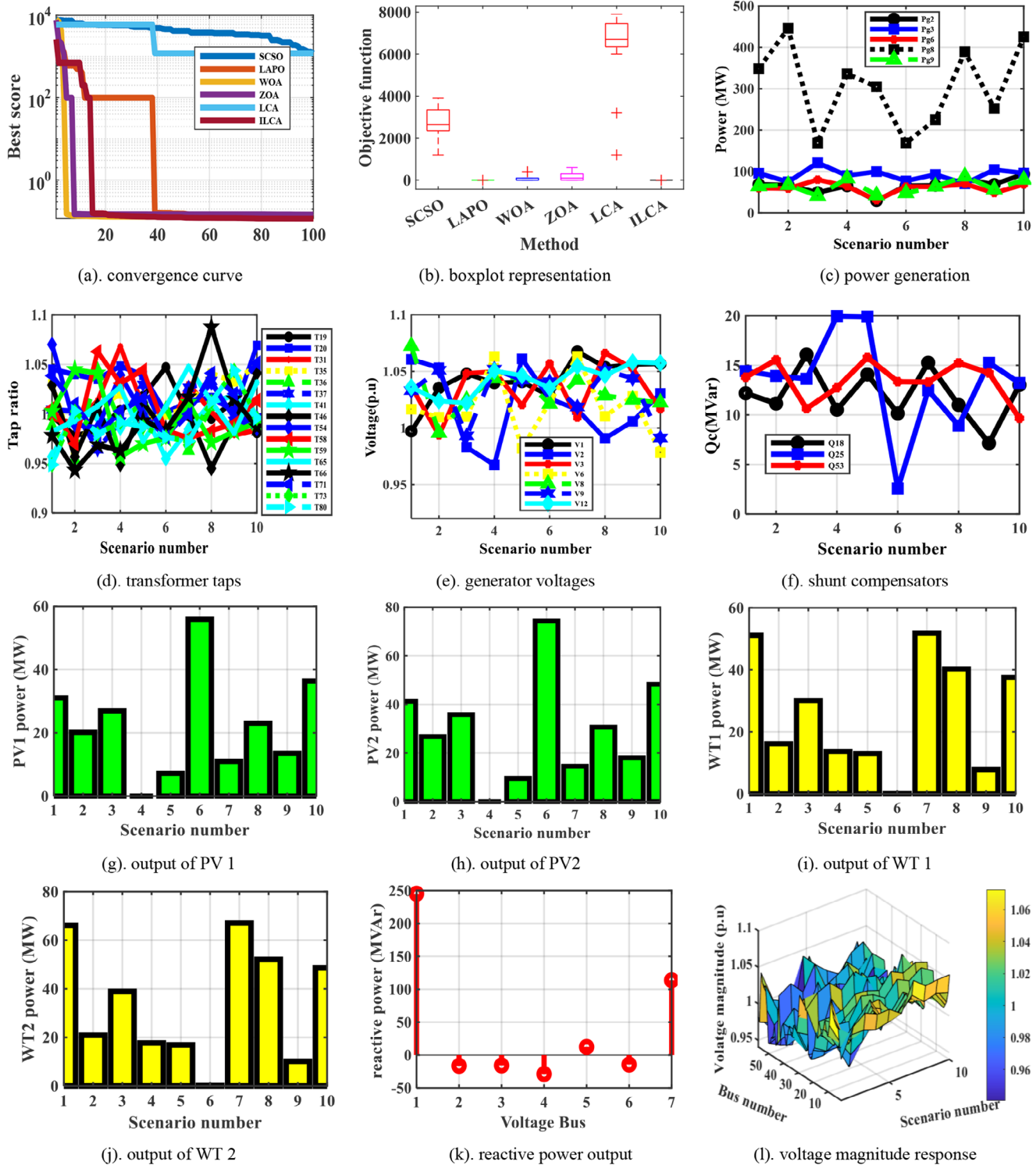
FIGURE 7 The response of system to enhance total predicted voltage stability index (TPSVI) with wind and PV resources.

6 | CONCLUSION

This paper resolved a stochastic optimal power flow frame-work considering modified RERs-based IEEE 57-bus stan-dard using an improved liver cancer algorithm (ILCA). The

proposed ILCA algorithm was successfully applied to the modified RERs-based IEEE 57-bus network to lessen the entire predicted loss and enhance the voltage stability. In the proposed ILCA, the four novel modifications were applied based on the Weibull flight operator, mutation-based

TABLE 9 The simulation results for objective of total predicted voltage stability index (TPVSI) with RESs.

Number of scenario	PL (MW)	TPPL (MW)	VSI (p.u)	TPVSI (p.u)
1	17.635291	0.017635	0.098769	0.000099
2	27.032889	0.675822	0.093802	0.002345
3	7.642022	0.053494	0.087133	0.000610
4	13.249578	6.664538	0.124529	0.062638
5	7.151824	1.745045	0.123442	0.030120
6	8.385536	0.008386	0.131582	0.000132
7	9.075609	1.025544	0.078700	0.008893
8	22.034528	0.308483	0.069505	0.000973
9	6.260091	0.563408	0.116576	0.010492
10	30.342511	0.060685	0.071775	0.000144
	TPPL (MW)	**11.1230 MW**	**TPVSI (p.u.)**	**0.1164 p.u.**

approach, quasi-opposite-based-learning (QOBL) and gorilla troops exploitation-based mechanisms to enhance the exploration and exploitation strengths of the traditional t-LCA. The statistical and non-parametric tests (Wilcoxon rank-sum and Friedman mean rank tests) were conducted on standard 23 benchmark functions, and the results verified the effectiveness of ILCA observed very competitive and has a rapid convergence response to reach the optimal solution almost in entire benchmark functions over to other traditional techniques like SCSO, LAPO, ZOA, WOA and t-LCA. The probability distribution function of produced power by RERs-based system was determined via Monte-Carlo simulation and reduction-based approaches. Moreover, using the system response with RERs-based modifications can save the entire predicted power loss to 32.6375%, while saving the entire predicted voltage stability index to 31.5294%, respectively. Future work can be extended by the incorporation of electric vehicles and storage systems in the network. Based on the obtained results, ILCA is a more effective and stable optimization algorithm that can be utilized to address a variety of optimization issues and is applicable in the renewable sector. Where, it may be employed to determine the best placement and ratings for renewable energy resources, as well as the distribution, transmission, microgrid, and nano-grid electrical systems.

NOMENCLATURE

b_m, l_n	Inequality and equality constraints
k, o	State and control variables
Q_C	Shunt VAR compensator
T	Transformer tap settings
P_{G2}	Active power from generator
V_G	Generator bus voltage
L_j	Line stability index of jth line.
N_{gs}	Number of created scenarios
Total_PPL	Expected predicted power losses
Total_PVSI	Total predicted voltage stability
PPL_n	Expected predicted power losses at n^{th} scenario
$PVSl_n$	Expected voltage stability at n^{th} scenario
NG	Number of generators
NC	Number of capacitor banks
R_{ld}	Loading used by normal PDF
X_{ci}	Certain solar irradiance
P_{RP}	Rated value for PV
$u_{\omega sr}, u_{\omega so}, u_{\omega si}$	Rated, cut-out and cut-in wind speed
T_L	Transmission line
P_{Loss}	Power losses
$\pi_{r,n}$	n^{th} scenario probability
V_j and V_i	Voltage at bus j and i
δ_{ij}	Voltage angle
G_{ij}	Conductance of transmission lines
Y_1 and Y_2	Bus admittance metrices
G_{ij}, B_{ij}	Conductance, susceptance of transmission line
P_{G1}	Slack bus
P_{Gi}, P_{Di}	Power generation and power demand
Q_{Gi}, Q_{Di}	Reactive power generation and demand
$\alpha_1, \alpha_2, \alpha_3, \alpha_4$	Penalty factors coefficients
NT	Number of transformers
NL	Number of loads connected
σ_{ld}, μ_{ld}	Mean and standard values for loading
σ_{sl}, μ_{sl}	Mean and the standard deviation
G_{ssi}	Standard solar irradiance values
β_{sp}, a_{sl}	Scale and shape parameters of Weibull PDF
P_{wrp}	Rated power of a wind turbine
VSI	Voltage stability index

AUTHOR CONTRIBUTIONS
Noor Habib Khan: Investigation; methodology; software; validation; writing—original draft. **Salman Habib**: Conceptualization; investigation; methodology; validation; visualization; writing—review and editing. **Raheela Jamal**: Validation; visualization; writing—review and editing. **Muhammad Majid Gulzar**: Resources; validation; writing—review and editing. **S. M. Muyeen**: Conceptualization; formal analysis; resources; writing—review and editing. **Mohamed Ebeed**: Data curation; writing—review and editing.

CONFLICT OF INTEREST STATEMENT
The authors declare no conflicts of interest.

DATA AVAILABILITY STATEMENT
Data is available on reasonable request.

ORCID

Noor Habib Khan 🄳 https://orcid.org/0000-0002-1007-9774
Muhammad Majid Gulzar 🄳 https://orcid.org/0000-0002-1091-3087
S. M. Muyeen 🄳 https://orcid.org/0000-0003-4955-6889
Mohamed Ebeed 🄳 https://orcid.org/0000-0003-2025-9821

REFERENCES

1. Ebeed, M., et al.: A modified artificial hummingbird algorithm for solving optimal power flow problem in power systems. Energy Rep. 11, 982–1005 (2024)
2. Mandal, B., Roy, P.K.: A probabilistic multi-objective approach for power flow optimization in hybrid wind-based power systems using grasshopper optimization algorithm. Int. J. Swarm Intell. Res. 11(4), 61–86 (2020)
3. Sabzevari, K., Habib, S., Sohrabi Tabar, V., Muaelou Shaillan, H., Hassan, Q., Muyeen, S.M.: Energy market trading in green microgrids under information vulnerability of renewable energies: A data-driven approach. Energy Rep. 11, 4467–4484 (2024). https://doi.org/10.1016/j.egyr.2024.03.059
4. Ebeed, M., Kamel, S., Jurado, F.: Optimal power flow using recent optimization techniques. In: Classical and Recent Aspects of Power System Optimization, pp. 157–183. Elsevier, Amsterdam (2018)
5. Jangir, P., Manoharan, P., Pandya, S., Sowmya, R.: MaOTLBO: Many-objective teaching-learning-based optimizer for control and monitoring the optimal power flow of modern power systems. Int. J. Ind. Eng. Comput. 14(2), 293–308 (2023)
6. Rizwan, P., Vikas, C., Manasa, Y.: Optimal power flow analysis and transmission system with jaya algorithm for reducing power loss. J. Syst. Eng. Electron. 34(3), (2024)
7. Ghasemi, M., Ghavidel, S., Ghanbarian, M.M., Massrur, H.R., Gharibzadeh, M.: Application of imperialist competitive algorithm with its modified techniques for multi-objective optimal power flow problem: A comparative study. Inf. Sci. 281, 225–247 (2014)
8. Hien, C.T., Duong, M.P., Pham, L.H.: Skill optimization algorithm for solving optimal power flow problem. Bull. Electr. Eng. Inf. 13(1), 12–19 (2024)
9. Qian, J., Wang, P., Chen, G.: Improved gravitational search algorithm and novel power flow prediction network for multi-objective optimal active dispatching problems. Expert Syst. Appl. 223, 119863 (2023)
10. Duman, S.: Solution of the optimal power flow problem considering FACTS devices by using lightning search algorithm. Iran. J. Sci. Technol. Trans. Electr. Eng. 43, 969–997 (2019)
11. Rosales Muñoz, A.A., Grisales-Noreña, L.F., Montano, J., Montoya, O.D., Perea-Moreno, A.-J.: Application of the multiverse optimization method to solve the optimal power flow problem in alternating current networks. Electronics 11(8), 1287 (2022)
12. Ali, A., et al.: A novel solution to optimal power flow problems using composite differential evolution integrating effective constrained handling techniques. Sci. Rep. 14(1), 6187 (2024)
13. Ebrahimi, A., Haghighi, R., Yektamoghadam, H., Dehghani, M., Nikoofard, A.: Optimal power flow by genetic algorithm. In: Frontiers in Genetics Algorithm Theory and Applications, pp. 121–136. Springer, Berlin, Heidelberg (2024)
14. Premkumar, M., Kumar, C., Dharma Raj, T., Sundarsingh Jebaseelan, S.D.T., Jangir, P., Haes Alhelou, H.: A reliable optimization framework using ensembled successive history adaptive differential evolutionary algorithm for optimal power flow problems. IET Gener. Transm. Distrib. 17(6), 1333–1357 (2023)
15. Guvenc, U., Duman, S., Kahraman, H.T., Aras, S., Katı, M.: Fitness–Distance Balance based adaptive guided differential evolution algorithm for security-constrained optimal power flow problem incorporating renewable energy sources. Appl. Soft Comput. 108, 107421 (2021)
16. Eberhart, R., Kennedy, J.: Particle swarm optimization. In: Proceedings of the IEEE International Conference on Neural Networks, vol. 4, pp. 1942–1948. IEEE, Piscataway, NJ (1995)
17. Khajeh, A., Modarress, H., Zeinoddini-Meymand, H.: Application of modified particle swarm optimization as an efficient variable selection strategy in QSAR/QSPR studies. J. Chemom. 26(11–12), 598–603 (2012)
18. Niknam, T., Zeinoddini Meymand, H., Doagou Mojarrad, H.: A novel multi-objective fuzzy adaptive chaotic PSO algorithm for optimal operation management of distribution network with regard to fuel cell power plants. Eur. Trans. Electr. Power 21(7), 1954–1983 (2011)
19. Firouzi, B.B., Meymand, H.Z., Niknam, T., Mojarrad, H.D.: A novel multi-objective chaotic crazy PSO algorithm for optimal operation management of distribution network with regard to fuel cell power plants. Int. J. Innov. Comput. I 7, 6395–6409 (2011)
20. Al-Kaabi, M., Dumbrava, V., Eremia, M.: Grey Wolf Optimizer for solving single objective functions optimal power flow. In: Proceedings of the 2023 13th International Symposium on Advanced Topics in Electrical Engineering (ATEE), pp. 1–5. IEEE, Piscataway, NJ (2023)
21. Mandal, B., Roy, P.K.: Multi-objective optimal power flow using grasshopper optimization algorithm. Optim. Control. Appl. Methods 45(2), 623–645 (2024)
22. Alam, M.K., Sulaiman, M.H.: Optimal power flow using moth-flame optimizer implementation. SSRN 4760595
23. Gupta, V.K., Mishra, S.K., Babu, R., Singh, A.K.: Solution of reactive power planning with TCSC and UPFC using improved Krill Herd algorithm. Trans. Indian Natl. Acad. Eng. 9(1), 87–99 (2024)
24. Chen, G., Qian, J., Zhang, Z., Li, S.: Application of modified pigeon-inspired optimization algorithm and constraint-objective sorting rule on multi-objective optimal power flow problem. Appl. Soft Comput. 92, 106321 (2020)
25. Jamal, R., et al.: Chaotic-quasi-oppositional-phasor based multi populations gorilla troop optimizer for optimal power flow solution. Energy 301, 131684 (2024)
26. Fu, X., Sun, H., Guo, Q., Pan, Z., Zhang, X., Zeng, S.: Probabilistic power flow analysis considering the dependence between power and heat. Appl. Energy 191, 582–592 (2017)
27. Ye, C.-J., Huang, M.-X.: Multi-objective optimal power flow considering transient stability based on parallel NSGA-II. IEEE Trans. Power Syst. 30(2), 857–866 (2014)
28. Habib, S., Kamarposhti, M.A., Shokouhandeh, H., Colak, I., Barhoumi, E.M.: Economic dispatch optimization considering operation cost and environmental constraints using the HBMO method. Energy Rep. 10, 1718–1725 (2023). https://doi.org/10.1016/j.egyr.2023.08.032
29. Sjöstrand, M., Aktaş, Ö.: Cornish-Fisher expansion and value-at-risk method in application to risk management of large portfolios. Thesis, Halmstad University. (2011)
30. Habib, S., Khan, M.M., Abbas, F., Ali, A., Hashmi, K., Shahid, M.U., Bo, Q., Tang, H.: Risk evaluation of distribution networks considering residential load forecasting with stochastic modeling of electric vehicles. Energy Technol. 7(7), 1900191 (2019). https://doi.org/10.1002/ente.201900191
31. Cao, J., Yan, Z.: Probabilistic optimal power flow considering dependences of wind speed among wind farms by pair-copula method. Int. J. Electr. Power Energy Syst. 84, 296–307 (2017)
32. Chen, J., Wu, Q., Zhang, L., Wu, P.: Multi-objective mean–variance–skewness model for nonconvex and stochastic optimal power flow considering wind power and load uncertainties. Eur. J. Oper. Res. 263(2), 719–732 (2017)
33. Zou, B., Xiao, Q.: Solving probabilistic optimal power flow problem using quasi Monte Carlo method and ninth-order polynomial normal transformation. IEEE Trans. on Power Syst. 29(1), 300–306 (2013)
34. Reddy, S.S.: Optimal power flow with renewable energy resources including storage. Electr. Eng. 99, 685–695 (2017)
35. Habib, S., Tamoor, M., Zaka, M.A., Jia, Y.: Assessment and optimization of carport structures for photovoltaic systems: A path to sustainable energy development. Energy Convers. Manage. 295, 117617 (2023). https://doi.org/10.1016/j.enconman.2023.117617
36. Agrawal, S., Pandya, S., Jangir, P., Kalita, K., Chakraborty, S.: A multi-objective thermal exchange optimization model for solving optimal power flow problems in hybrid power systems. Decis. Anal. J. 8, 100299 (2023)

37. Ashour, A., Alkhaldi, T.M.: Optimal power flow considering wind integration using anti lion optimization algorithm. Int. J. Eng. Res. Appl. 11(11), 17–25 (2024)

38. Panda, A., Tripathy, M.: Security constrained optimal power flow solution of wind-thermal generation system using modified bacteria foraging algorithm. Energy 93, 816–827 (2015)

39. Li, S., Gong, W., Wang, L., Yan, X., Hu, C.: Optimal power flow by means of improved adaptive differential evolution. Energy 198, 117314 (2020)

40. Ramesh, M., Swarnasri, K., Muthukumar, P., Babu, P.V.K.: Improved skill optimization algorithm based optimal power flow considering open-access trading of wind farms and electric vehicle fleets. Int. J. Intell. Eng. Syst. 17(2), 402–411 (2024)

41. Naidu, T., Balasubramanian, G., Rao, B.V.: Optimal power flow with distributed energy sources using whale optimization algorithm. Int. J. Electr. Comput. Eng. 13(5), 4835–4844 (2023).

42. Nemouchi, W., Amrane, Y., Kouba, N.E.Y., Boucetta, L.N., Nemouchi, H.: Multi-objective optimal power flow considering offshore wind farm. In: Frontiers in Genetics Algorithm Theory and Applications, pp. 137–156. Springer, Berlin, Heidelberg (2024)

43. Khan, N.H., Jamal, R., Ebeed, M., Kamel, S., Zeinoddini-Meymand, H., Zawbaa, H.M.: Adopting Scenario-Based approach to solve optimal reactive power dispatch problem with integration of wind and solar energy using improved marine predator algorithm. Ain Shams Eng. J. 13(5), 101726 (2022)

44. Kamel, S., Ebeed, M., Jurado, F.: An improved version of salp swarm algorithm for solving optimal power flow problem. Soft Comput. 25(5), 4027–4052 (2021)

45. Taher, M.A., Kamel, S., Jurado, F., Ebeed, M.: An improved moth-flame optimization algorithm for solving optimal power flow problem. Int. Trans. Electr. Energy Syst. 29(3), e2743 (2019)

46. Zobaa, A.F., Aleem, S.A.: Uncertainties in Modern Power Systems. Academic Press, Cambridge, MA (2020)

47. Ebeed, M., Alhejji, A., Kamel, S., Jurado, F.: Solving the optimal reactive power dispatch using marine predators algorithm considering the uncertainties in load and wind-solar generation systems. Energies 13(17), 4316 (2020)

48. Morshed, M.J., Hmida, J.B., Fekih, A.: A probabilistic multi-objective approach for power flow optimization in hybrid wind-PV-PEV systems. Appl. Energy 211, 1136–1149 (2018)

49. Abdullah, M., Javaid, N., Khan, I.U., Khan, Z.A., Chand, A., Ahmad, N.: Optimal power flow with uncertain renewable energy sources using flower pollination algorithm. In: Proceedings of the International Conference on Advanced Information Networking and Applications, pp. 95–107. Springer, Cham (2019)

50. Houssein, E.H., Oliva, D., Samee, N.A., Mahmoud, N.F., Emam, M.M.: Liver Cancer Algorithm: A novel bio-inspired optimizer. Comput. Biol. Med. 165, 107389 (2023)

51. Price, K., Storn, R.M., Lampinen, J.A.: Differential Evolution: A Practical Approach to Global Optimization. Springer Science & Business Media, Berlin, Heidelberg (2006)

52. Mallipeddi, R., Suganthan, P.N., Pan, Q.-K., Tasgetiren, M.F.: Differential evolution algorithm with ensemble of parameters and mutation strategies. Appl. Soft Comput. 11(2), 1679–1696 (2011)

53. Xu, Q., Wang, L., Wang, N., Hei, X., Zhao, L.: A review of opposition-based learning from 2005 to 2012. Eng. Appl. Artif. Intell. 29, 1–12 (2014)

54. Lenin, K.: Quasi opposition-based quantum Pieris rapae and parametric curve search optimization for real power loss reduction and stability enhancement. IEEE Trans. Ind. Appl. 59(3), 3077–3085 (2023)

55. Li, Y., Wang, G.: Sand cat swarm optimization based on stochastic variation with elite collaboration. IEEE Access 10, 89989–90003 (2022)

56. Khan, N.H., et al.: A novel modified lightning attachment procedure optimization technique for optimal allocation of the FACTS devices in power systems. IEEE Access 9, 47976–47997 (2021)

57. Trojovská, E., Dehghani, M., Trojovský, P.: Zebra optimization algorithm: A new bio-inspired optimization algorithm for solving optimization algorithm. IEEE Access 10, 49445–49473 (2022)

58. Zhao, W., et al.: Electric eel foraging optimization: A new bio-inspired optimizer for engineering applications. Expert Syst. Appl. 238, 122200 (2024)

59. Jamal, R., et al.: Chaotic-quasi-oppositional-phasor based multi populations gorilla troop optimizer for optimal power flow solution. Energy 301, 131684 (2024)

60. Khan, N.H., et al.: A novel modified artificial rabbit optimization for stochastic energy management of a grid-connected microgrid: A case study in China. Energy Rep. 11, 5436–5455 (2024)

61. Bakir, H.: Optimal power flow analysis with circulatory system-based optimization algorithm. Turkish J. Eng. 8(1), 92–106 (2024)

APPENDICES

TABLE A1 Benchmark unimodal functions.

Formulation of function	Range limit	$Func_{\min}$
$f_1(k) = \sum_{j=1}^{n} k_j^2$	$[-100, 100]$	0
$f_2(k) = \sum_{j=1}^{n} |k_j| + \prod_{j=1}^{n} |k_j|$	$[-10, 10]$	0
$f_3(k) = \sum_{j=1}^{n} \left(\sum_{i-1}^{j} k_i\right)^2$	$[-100, 100]$	0
$f_4(k) = \max_j |k_j|, 1 \leq j \leq n$	$[-100, 100]$	0
$f_5(k) = \sum_{j=1}^{n-1}[100(k_{j+1} - k_j^2)^2 + (k_j - 1)^2]$	$[-30, 30]$	0
$f_6(k) = \sum_{j=1}^{n-1} ([k_j + 0.5])^2$	$[-100, 100]$	0
$f_7(k) = \sum_{j=1}^{n} jk_j^4 + random(0, 1)$	$[-1.28, 1.28]$	0

TABLE A2 Benchmark multi-modal functions.

Formulation of function	Range limit	$Func_{min}$
$f_8(k) = \sum_{j=1}^{n} -k_j \sin(\sqrt{|k_j|})$	$[-500, 500]$	-418.9829×5
$f_9(k) = \sum_{j=1}^{n} [k_j^2 - 10\cos(2\pi k_j + 10)]$	$[-5.12, 5.12]$	0
$f_{10}(k) = -20\exp\left(-0.2\sqrt{\frac{1}{n}\sum_{j=1}^{n} k_j^2}\right) - \exp\left(\frac{1}{n}\sum_{j=1}^{n}\cos(2\pi k_j) + 20 + e\right)$	$[-32, 32]$	0
$f_{11}(k) = \frac{1}{4000}\sum_{j=1}^{n} k_j^2 - \prod_{j=1}^{n}\cos\left(\frac{k_j}{\sqrt{j}}\right) + 1$	$[-600, 600]$	0
$f_{12}(k) = \frac{\pi}{n}\{10\sin(\pi z_1) + \sum_{j=1}^{n-1}(z_j - 1)^2[1 + 10\sin^2(\pi z_{j+1})] + (z_n - 1)^2\} + \sum_{j=1}^{n} u(k_j, 10, 100, 4)$	$[-50, 50]$	0
$z_j = 1 + \frac{k_j + 1}{4}$		
$u(k_j, v, s, h) = \begin{cases} x(k_j - v)^b & k_j > v \\ 0 - v < k_j < v \\ x(-k_j - v)^b & k_j < -v \end{cases}$		
$f_{13}(k) = 0.1\{\sin^2(3\pi k_1) + \sum_{j=1}^{n}(k_j - 1)^2[1 + \sin^2(3\pi k_j + 1)] + (k_n - 1)^2[1 + \sin^2(2\pi k_j)]\} + \sum_{j=1}^{n} u(k_j, 5, 100, 4)$	$[-50, 50]$	
$f_{14}(k) = -\sum_{j=1}^{n}\sin(k_j) \cdot \left(\sin\left(\frac{j \cdot k_j^2}{\pi}\right)\right)^{2b}, b = 10$	$(0, \pi)$	-4.687
$f_{15}(k) = \left[e^{-\sum_{j=1}^{n}\left(\frac{k_j}{\beta}\right)^{2b}} - 2e^{-\sum_{j=1}^{n} k_j^2}\right] - \prod_{j=1}^{n}\cos^2 k_j, b = 5$	$[-20, 20]$	-1
$f_{16}(k) = \left\{\left[\sum_{j=1}^{n}\sin^2(k_j)\right] - \exp\left(-\sum_{j=1}^{n} k_j^2\right)\right\} \cdot \exp\left[-\sum_{j=1}^{n}\sin^2\sqrt{|k_j|}\right]$	$[-10, 10]$	-1

TABLE A3 Benchmark fixed-dimensional multi-modal functions.

Formulation of function	Dim	Range limit	$Func_{min}$
$f_{14}(k) = \frac{1}{500} + \sum_{i=1}^{25}\frac{1}{i + \sum_{j=1}^{2}(k_j - a_{ji})^6}$	2	$[-65, 65]$	1
$f_{15}(k) = \sum_{j=1}^{11}\left[b_j - \frac{k_j(b_j^2 + b_j k_2)}{b_j^2 + b_j k_{3+} k_4}\right]^2$	4	$[-5, 5]$	0.00030
$f_{16}(k) = 4k_1^2 - 2.1k_1^4 + \frac{1}{3}k_1^6 + k_1 k_2 - 4k_2^2 + 4k_2^4$	2	$[-5, 5]$	-1.0316
$f_{17}(k) = \left(k_2 - \frac{5.1}{4\pi^2}k_1^2 + \frac{5}{\pi}k_1 - 6\right)^2 + 10\left(1 - \frac{1}{8\pi}\right)\cos k_1 + 10$	2	$[-5, 5]$	0.398
$f_{18}(k) = \left[1 + (k_1 + k_2 + 1)^2\left(19 - 14k_1 + 3k_1^2 - 14k_2 + 6k_1 k_2 + 3k_2^2\right)\right]$ $* \left[30 + (2k_1 - 3k_2)^2\left(18 - 32k_1 + 12k_1^2 - 48k_2 + 36k_1 k_2 + 27k_2^2\right)\right]$	2	$[-2, 2]$	3
$f_{19}(k) = -\sum_{j=1}^{4} c_j \exp\left(-\sum_{i=1}^{3} a_{ji}(k_i - p_{ji})^2\right)$	3	$[1, 3]$	3.86-
$f_{20}(k) = -\sum_{j=1}^{4} c_j \exp\left(-\sum_{i=1}^{6} a_{ji}(k_i - p_{ji})^2\right)$	6	$[0, 1]$	-3.32
$f_{21}(k) = -\sum_{j=1}^{5}\left[(k - a_j)(k - a_j)^T + c_j\right]^{-1})$	4	$[0, 10]$	-10.1532
$f_{22}(k) = -\sum_{j=1}^{7}\left[(k - a_j)(k - a_j)^T + c_j\right]^{-1})$	4	$[0, 10]$	-10.4028
$f_{23}(k) = -\sum_{j=1}^{10}\left[(k - a_j)(k - a_j)^T + c_j\right]^{-1})$	4	$[0, 10]$	-10.5363